

Classification of bifurcation diagrams in coupled phase-oscillator models with asymmetric natural frequency distributions

Ryosuke Yoneda¹ and Yoshiyuki Y. Yamaguchi²

^{1,2}Graduate School of Informatics, Kyoto University, Kyoto 606-8501, Japan

E-mail: ¹ yonedaryosuke@amp.i.kyoto-u.ac.jp and ² yyama@amp.i.kyoto-u.ac.jp

Abstract. Synchronization among rhythmic elements is modeled by coupled phase-oscillators each of which has the so-called natural frequency. The natural frequency distribution determines types of bifurcation diagrams, which contain continuous or discontinuous synchronization transitions from the nonsynchronized state for instance. It has been numerically reported that asymmetry in the natural frequency distributions brings new types of bifurcation diagrams having oscillation or a discontinuous jump of the order parameter which emerge from partially synchronized states. We propose a theoretical classification method of five types of bifurcation diagrams including the new ones paying attention to generality of the theory. The oscillation and the jump from partially synchronized states are discussed respectively by the linear analysis around the nonsynchronized state and by extending the amplitude equation up to the third leading term. The theoretical classification is examined by comparing with numerical results.

Submitted to: *J. Phys. A: Math. Theor.*

1. Introduction

Synchronization among rhythmic elements is observed in various fields of nature such as metronomes [1], flashing of fireflies [2, 3], frog choruses [4], and Josephson junction arrays [5, 6]. The synchronization is modeled by coupled phase-oscillators [7, 8], which produce the collective rhythm if the strength of couplings, represented by the coupling constant, is sufficiently large. It is, therefore, one of central issues in the coupled oscillator systems to reveal bifurcation diagrams, which describe the relation between the coupling constant and the extent of synchronicity.

The Kuramoto model [8] is a paradigmatic coupled phase-oscillator model, whose couplings are described by the single sinusoidal coupling function. Each phase-oscillator has the so-called natural frequency following the natural frequency distribution and this distribution determines types of bifurcation diagrams. If the natural frequency distribution is symmetric and unimodal, the synchronization transition is continuous [8, 9, 10]. In other words, the order parameter, representing the extent of synchronization, continuously varies at the critical point as the coupling constant gets large. Extending the natural frequency distribution from unimodal to bimodal, we find discontinuous transitions and temporal oscillations of the order parameter [11].

A major part of previous studies assumed symmetry of the natural frequency distributions as mentioned above. However, it has been recently reported that asymmetry brings new types of bifurcation diagrams [12]. As the strength of couplings increases, a continuous synchronization transition happens first, and after that, a discontinuous jump or oscillation of the order parameter emerges. These new types of bifurcation diagrams have been obtained by performing numerical simulations. The purpose of this paper is to propose a theoretical criterion to classify the bifurcation diagrams for a family of natural frequency distributions including both symmetric and asymmetric ones.

The Kuramoto model is one of the simplest models to obtain several bifurcation diagrams, but the single sinusoidal coupling function is not always the case [13, 14, 15]. The theory must be, therefore, applicable to general systems beyond the Kuramoto model. Keeping this point in mind, we review three theoretical methods which analyze bifurcation diagrams and which are based on the large population limit described by the equation of continuity.

The first method is the self-consistent equation for the order parameter [8, 9]. The mean-field nature of the Kuramoto model permits to write the stationary solutions to the equation of continuity by using an unknown value of the order parameter. A stationary value of the order parameter is obtained by using the stationary solution and the unknown order parameter is determined self-consistently. The self-consistent strategy is useful because it provides a nonlinear analysis. However, if the coupling function contains higher-order harmonics, there may exist several stable locking phases for a given natural frequency and this method requires to compute the distribution of oscillators over the stable phases [16, 17]. Moreover, oscillating states are not captured by this method.

The second method is the Ott-Antonsen ansatz [18, 19]. This ansatz reduces the equation of continuity associated with the Kuramoto model to a few dimensional ordinary differential equation. Consequently, the classification problem is simplified into the classification in the reduced systems [11]. This method is powerful in the Kuramoto model and its variances having a single sinusoidal coupling function, but

is not applicable for other coupled-oscillators systems, which have generic coupling functions. Moreover, the reduction is successful for special families of natural frequency distributions like rational functions including Lorentzians. The Gaussian distribution is not suitable for instance. Even if the distribution consists of some Lorentzians, the dimension of the reduced system becomes higher and the stationary point analysis becomes harder as the number of Lorentzians increases.

We, therefore, adopt the third method of the amplitude equation [20]. The idea of this method is to project dynamics onto the unstable manifold of the nonsynchronized stationary state, and to consider temporal evolution of amplitude of the unstable eigenfunctions. In contrast to the previous two methods, this method is widely useful in the Kuramoto model [20], in a coupled phase-oscillators with a generic coupling function [21], in an extended Kuramoto model with inertia [22], and in Hamiltonian systems [23, 24]. The amplitude equation is constructed perturbatively and has been usually truncated up to the second leading term, since it is sufficient to judge continuity of the synchronization transition. To capture the jump from partially synchronized states, we extend the amplitude equation up to the third leading term. For the amplitude equation, the linear analysis around the nonsynchronized state is a basic block, and it is also useful to capture the stability of the nonsynchronized state and the oscillation of the order parameter. Another crucial advantage is that this method is applicable to any forms of natural frequency distributions including asymmetric ones and nonrational ones.

We underline that the method proposed in this paper is in principle applicable to general systems beyond the Kuramoto model and its variances. Nevertheless, we investigate the Kuramoto model to illustrate usefulness of the method. One reason is that the new types of bifurcation diagrams are reported in the Kuramoto model and we give a theoretical explanation of this previous work [12]. Another reason is that, as we discussed above, the reduction by the Ott-Antonsen ansatz permits us to obtain numerically a precise classification, which helps to examine the theory.

This paper is organized as follows. In Sec. 2, we introduce the Kuramoto model and its large population limit written by the equation of continuity. A considering family of the natural frequency distribution, which is characterized by two parameters, is also exhibited. In Sec. 3, we divide numerically the parameter space into five domains corresponding to types of bifurcation diagrams and prepare the reference parameter space to examine the theory. This numerical search is performed by using the Ott-Antonsen reduction. We stress that this reduction is used solely for obtaining the reference parameter space and is not used in our theory. In Sec. 4, a linear and a nonlinear analyses of the equation of continuity are shortly reviewed. With the aid of these analyses, we propose the ideas to identify the domains on the parameter space and report the consequence of the theory in Sec. 5. Finally, we summarize this paper in Sec. 6.

2. Model

The Kuramoto model is expressed by the N -dimensional ordinary differential equation,

$$\frac{d\theta_j}{dt} = \omega_j - \frac{K}{N} \sum_{k=1}^N \sin(\theta_j - \theta_k), \quad (j = 1, \dots, N). \quad (1)$$

The real constant $K > 0$ is the coupling constant, $\theta_j \in (-\pi, \pi] = \mathbb{S}^1$ and $\omega_j \in \mathbb{R}$ are respectively the phase and the natural frequency of the j th oscillator. The natural

frequencies ω_j obey a probability distribution function $g(\omega)$. We introduce a family of $g(\omega)$ as

$$g(\omega) = \frac{C}{[(\omega - \Omega)^2 + \gamma_1^2][(\omega + \Omega)^2 + \gamma_2^2]} \quad (2)$$

to systematically consider unimodal and bimodal, and symmetric and asymmetric distributions [12, 25]. The family of $g(\omega)$ consists of rational functions, which is useful to draw the reference parameter space by using the Ott-Antonsen ansatz, but is not crucial in our methodology. Here,

$$C = \frac{\gamma_1 \gamma_2 [(\gamma_1 + \gamma_2)^2 + 4\Omega^2]}{\pi(\gamma_1 + \gamma_2)} \quad (3)$$

is obtained by the normalization condition

$$\int_{-\infty}^{\infty} g(\omega) d\omega = 1. \quad (4)$$

All the parameters γ_1, γ_2 , and Ω are assumed to be positive. By scaling the variables t, ω_j, K , and γ_1 , we can set $\gamma_2 = 1$ without loss of generality. Thus, the family of $g(\omega)$ is characterized by a point on the parameter space (γ_1, Ω) . Moreover, by putting $\theta \rightarrow -\theta$, we may restrict the parameter γ_1 to $\gamma_1 \leq 1$. The line $\gamma_1 = 1$ gives a family of symmetric distributions.

The complex order parameter z is defined by

$$z = r e^{i\psi} = \frac{1}{N} \sum_{j=1}^N e^{i\theta_j}, \quad (r, \psi \in \mathbb{R}). \quad (5)$$

The absolute value r measures the extent of synchronization. If all the oscillators distribute uniformly on \mathbb{S}^1 , then $r \simeq 0$. If $r \simeq 1$, the majority of oscillators gathers around a point on \mathbb{S}^1 .

In the limit of large population $N \rightarrow \infty$, by the conservation of the number of oscillators, the equation of motion Equation (1) can be written in the equation of continuity [26],

$$\frac{\partial F}{\partial t} + \frac{\partial}{\partial \theta} (v[F]F) = 0, \quad (6)$$

$$v[F] = \omega - K \int_{-\infty}^{\infty} d\omega' \int_{-\pi}^{\pi} d\theta' \sin(\theta - \theta') F(\theta', \omega', t), \quad (7)$$

$$(8)$$

where $F(\theta, \omega, t)$ is the probability distribution function of θ and ω at time t . In other words, $F(\theta, \omega, t) d\theta d\omega$ represents the fraction of oscillators having phases between θ and $\theta + d\theta$ and natural frequencies between ω and $\omega + d\omega$ at the time t . From the normalization condition $\int F d\theta d\omega = 1$, we have

$$\int_{-\pi}^{\pi} F(\theta, \omega, t) d\theta = g(\omega). \quad (9)$$

In this limit the order parameter is expressed by

$$z = r e^{i\psi} = \int_{-\infty}^{\infty} d\omega \int_{-\pi}^{\pi} d\theta F(\theta, \omega, t) e^{i\theta}. \quad (10)$$

3. Numerical Classification on Parameter space

The aim of this section is to classify numerically the parameter space (γ_1, Ω) into five types of bifurcation diagrams [25] before developing a theoretical criterion. The direct N -body simulations of the model Equation (1) include finite-size fluctuation, which makes it difficult to judge the types of bifurcation diagrams. We, therefore, consider the equation of continuity Equation (8) for eliminating the finite-size fluctuation. Further, in the Kuramoto model, the Ott-Antonsen ansatz [18, 19] reduces the infinite-dimensional partial differential equation Equation (8) to a real four-dimensional ordinary differential equation for the considering family of natural frequency distributions Equation (2).

The Ott-Antonsen ansatz is a special technique to the Kuramoto model and some variants. This ansatz is used for performing the classification of the parameter space which is compared with the one obtained by the theoretical criterion presented later. We underline that the proposed theoretical method is applicable for other generic models and for any natural frequency distributions in principle.

3.1. Ott-Antonsen reduction

The reduced equation by using the Ott-Antonsen ansatz is expressed as [12]

$$\frac{dz_1}{dt} = (i\Omega - \gamma_1)z_1 - \frac{K}{2}(z_1^* z_1^2 - z), \quad (11)$$

$$\frac{dz_2}{dt} = -(i\Omega + \gamma_2)z_2 - \frac{K}{2}(z_2^* z_2 - z). \quad (12)$$

The two variables z_1 and z_2 are complex and the complex order parameter z is written as

$$z = k_1 z_1 + k_2 z_2$$

with the complex constants k_1 and k_2 defined by

$$k_1 = \frac{\gamma_2[2\Omega - i(\gamma_1 + \gamma_2)]}{(\gamma_1 + \gamma_2)[2\Omega + i(\gamma_1 - \gamma_2)]}, \quad (13)$$

$$k_2 = \frac{\gamma_1[2\Omega + i(\gamma_1 + \gamma_2)]}{(\gamma_1 + \gamma_2)[2\Omega + i(\gamma_1 - \gamma_2)]}. \quad (14)$$

In the later computations we set $\gamma_2 = 1$ without loss of generality as we mentioned in the previous section 2, but we kept γ_2 free to show the dependence explicitly. See Appendix Appendix A for details of the reduction.

3.2. Bifurcation diagrams

Numerical integration of the reduced system Equation (12) is performed by using the fourth-order Runge-Kutta algorithm with the time step $\Delta t = 0.01$. For a given set of (γ_1, Ω) , we start from $K = 0$ and increase the value up to $K = 10$ with the step $\Delta K = 0.01$. This increasing process is called the forward process. At each K , the time average and standard deviation of the order parameter are taken in the time interval $t \in [4500, 5000]$ to avoid a transient regime. The final state at $t = 5000$ is used as the initial state at the successive value of K . If the final state is the origin, then we shift the initial state from the origin to $z_1 = z_2 = 0.01$ to escape from the trivial stationary state. After arriving $K = 10$, we decrease the value of K from $K = 10$ to $K = 0$ to

check appearance of the hysteresis which reveals the discontinuous transition. This decreasing process is called the backward process.

The parameter space (γ_1, Ω) is classified into five domains as shown in Fig. 1 [25]. The five domains correspond to the five types of bifurcation diagrams reported in Fig. 2. In particular, the symmetry line $\gamma_1 = 1$ is classified into the three intervals included in A, B, and C. The separating points $\Omega = 1$ and $\sqrt{3}$ are obtained by applying the amplitude equation and the eigenvalue analysis respectively, which are explained later. The asymmetry region $\gamma_1 < 1$ includes the new domains D and E with the known domains of A and B. The goal of this paper is to reproduce the parameter space theoretical

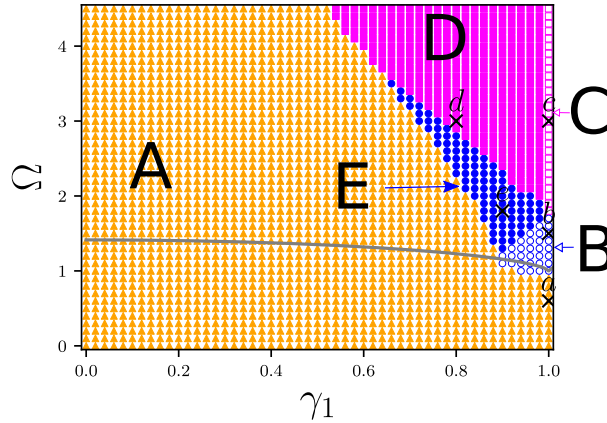


Figure 1. Classification of the parameter space (γ_1, Ω) into the five domains: A (filled orange triangles), B (open blue circles), C (open magenta squares), D (filled magenta squares), and E (filled blue circles). This classification is obtained by performing numerical simulations of the reduced system Equation (12). The gray line represents the borderline between the unimodal and bimodal natural frequency distributions $g(\omega)$. The bifurcation diagrams at the five points marked by the crosses are reported in Fig. 2.

4. Theoretical analyses of equation of continuity

We shortly review a linear and a nonlinear analyses of the equation of continuity Equation (8) around the nonsynchronized state f^0 , which is explicitly written as

$$f^0(\omega) = \frac{g(\omega)}{2\pi}. \quad (15)$$

It is straightforward to check stationarity of f^0 as

$$\frac{\partial}{\partial \theta}(v[f^0]f^0) = 0 \quad (16)$$

from the fact $v[f^0] = \omega$. We expand the equation of continuity by substituting

$$F(\theta, \omega, t) = f^0(\omega) + f(\theta, \omega, t). \quad (17)$$

The equation for the perturbation f is written as

$$\frac{\partial f}{\partial t} = \mathcal{L}f + \mathcal{N}[f], \quad (18)$$

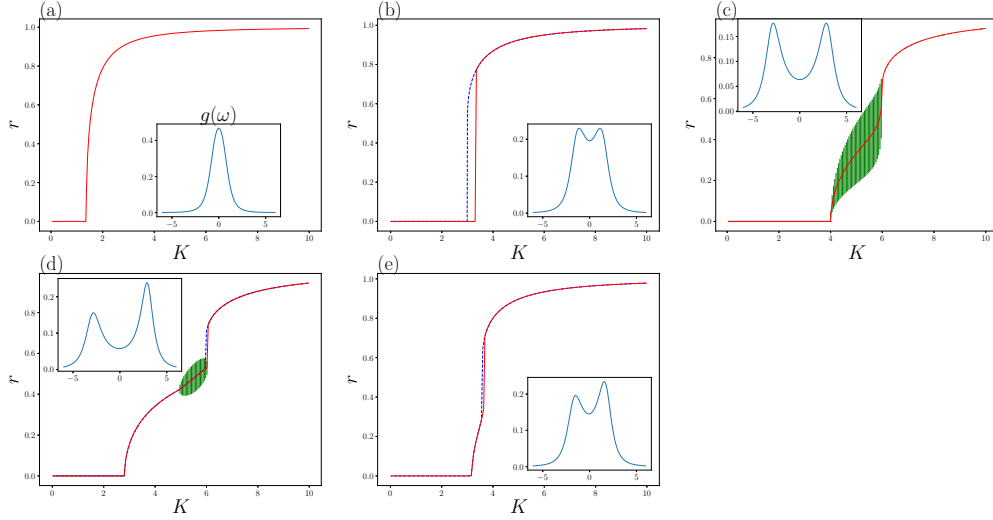


Figure 2. Five bifurcation diagrams at the five points marked on the parameter space in Fig. 1. The values of parameters (γ_1, Ω) are (a) (1.0, 0.6), (b) (1.0, 1.5), (c) (1.0, 3.0), (d) (0.8, 3.0), and (e) (0.9, 1.8). The forward process (red solid line) and the backward process (blue dashed line). In the panels (a) and (c), the backward line collapses with the forward line. The standard deviations of the order parameter are represented by the vertical bars, but they are not visible in (a), (b), and (e). The insets show the natural frequency distributions $g(\omega)$ against ω .

where the linear part is

$$\mathcal{L}f = -\omega \frac{\partial f}{\partial \theta} + K f^0 \frac{\partial}{\partial \theta} \int_{-\infty}^{\infty} d\omega' \int_{-\pi}^{\pi} d\theta' \sin(\theta - \theta') f(\theta', \omega', t) \quad (19)$$

and the nonlinear part is

$$\mathcal{N}[f] = K \frac{\partial}{\partial \theta} \left[f \int_{-\infty}^{\infty} d\omega' \int_{-\pi}^{\pi} d\theta' \sin(\theta - \theta') f(\theta', \omega', t) \right]. \quad (20)$$

Note that the equation Equation (18) is an exact transform from the equation of continuity Equation (8).

4.1. Linear analysis

Any functions of θ are expanded into the Fourier series as

$$f(\theta, \omega, t) = \sum_{k \in \mathbb{Z}} \tilde{f}_k(\omega, t) e^{ik\theta}. \quad (21)$$

The linear analysis can be performed independently in each Fourier mode k , because the nonsynchronized state $f^0(\omega)$ does not depend on θ . In the Kuramoto model providing the linear part Equation (19), the Fourier modes $k \neq \pm 1$ give solely rotations and instability comes from the modes $k = \pm 1$. The eigenvalues for the modes $k = \pm 1$ are obtained as roots of the spectral functions

$$\Lambda_{\pm 1}(\lambda) = 1 - \frac{K}{2} \int_{-\infty}^{\infty} \frac{g(\omega)}{\lambda \pm i\omega} d\omega. \quad (22)$$

See Appendix Appendix B for details. If the real part of a root is positive, the eigenvalue induces instability. We call such an eigenvalue as an unstable eigenvalue, which is the target of the amplitude equation introduced in the next subsection 4.2.

The nonsynchronized state f^0 changes the stability at the synchronization transition point K_c . Naïvely saying, the eigenvalue having the largest real part must pass the imaginary axis at K_c . However, the integrands of the spectral functions $\Lambda_{\pm 1}(\lambda)$ have singularities at $\omega = \pm i\lambda$, which are on the integral contour, the real axis, if λ is pure imaginary. To avoid these singularities and to observe K dependence of the eigenvalues, we perform the analytic continuation of $\Lambda_{\pm 1}(\lambda)$. The continued functions are denoted by $D_{\pm 1}(\lambda)$. See Appendix Appendix C for the continuation.

We give three remarks. First, a root of $D_{\pm 1}(\lambda)$ may not be an eigenvalue if the real part of the root is nonpositive. We call a root of $D_{\pm 1}(\lambda)$ as a fake eigenvalue. Second, nevertheless, a root of $D_{\pm 1}(\lambda)$ whose real part is positive is also a root of $\Lambda_{\pm 1}(\lambda)$. Therefore, we do not need to introduce the term of unstable fake eigenvalue. Third, the relations

$$\Lambda_{-1}(\lambda^*) = \Lambda_1^*(\lambda) \quad (23)$$

and

$$D_{-1}(\lambda^*) = D_1^*(\lambda) \quad (24)$$

hold, where $\Lambda_1^*(\lambda) = [\Lambda_1(\lambda)]^*$ for instance and $[\Lambda_1(\lambda)]^*$ is the complex conjugate of $\Lambda_1(\lambda)$. These relations imply that λ^* is a (fake) eigenvalue if λ is so.

For the family of natural frequency distributions Equation (2), the equation $D_1(\lambda) = 0$ leads a quadratic equation of λ and has the two roots of λ_1 and λ_2 with $\text{Re}(\lambda_1) \geq \text{Re}(\lambda_2)$. In this paper, the two fake eigenvalues λ_1 and λ_2 are called the first and the second fake eigenvalues respectively. See Appendix Appendix D for the quadratic equation of λ , the determination of the critical point K_c , and the number of unstable eigenvalues.

4.2. Amplitude equation

We assume that the linear operator \mathcal{L} has only one pair of unstable eigenvalues, λ_1 and λ_1^* , whose corresponding eigenfunctions are $\Psi(\theta, \omega)$ and $\Psi^*(\theta, \omega)$ respectively. To derive the amplitude equation, we expand f into

$$f(\theta, \omega, t) = A(t)\Psi(\theta, \omega) + A^*(t)\Psi^*(\theta, \omega) + H(\theta, \omega, A, A^*). \quad (25)$$

The amplitude A relates to the order parameter z as

$$z = 2\pi A^* + O(|A|^3). \quad (26)$$

The asymptotic value of z is, therefore, approximately obtained by considering temporal evolution of the amplitude $A(t)$. The function H represents the unstable manifold of the nonsynchronized state f^0 . In other words, H represents the height of the unstable manifold from the eigenspace $\text{Span}\{\Psi, \Psi^*\}$. We assume that the unstable manifold is tangent to the eigenspace $\text{Span}\{\Psi, \Psi^*\}$ and $H = O(|A|^2)$.

For deriving the amplitude equation, we introduce the adjoint linear operator \mathcal{L}^\dagger of \mathcal{L} which is defined by

$$(\mathcal{L}^\dagger f_1, f_2) = (f_1, \mathcal{L} f_2), \quad \text{for } \forall f_1, f_2. \quad (27)$$

The inner product is defined by

$$(f_1, f_2) = \int_{-\infty}^{\infty} d\omega \int_{-\pi}^{\pi} d\theta f_1^*(\theta, \omega) f_2(\theta, \omega). \quad (28)$$

We can compute the eigenfunctions of \mathcal{L}^\dagger , $\tilde{\Psi}$ and $\tilde{\Psi}^*$, which correspond to the eigenvalues λ_1^* and λ_1 respectively. See Appendix Appendix E for details.

Let us assume the orthogonality

$$\left(\tilde{\Psi}, H\right) = \left(\tilde{\Psi}^*, H\right) = 0. \quad (29)$$

We can choose the eigenfunctions satisfying the relations

$$\left(\tilde{\Psi}, \Psi\right) = 1, \quad \left(\tilde{\Psi}, \Psi^*\right) = 0, \quad (30)$$

$$\left(\tilde{\Psi}^*, \Psi\right) = 0, \quad \left(\tilde{\Psi}^*, \Psi^*\right) = 1, \quad (31)$$

without loss of generality. Substituting the expansion Equation (25) into the equation of continuity Equation (8) and using the relations Equation (29) and Equation (31), we have the equation for the amplitude A as

$$\frac{dA}{dt} = \lambda_1 A + \left(\tilde{\Psi}, \mathcal{N}[f]\right) \quad (32)$$

and the equation for the unstable manifold H as

$$\frac{dH}{dt} = \mathcal{L}H + \mathcal{N}[f] - \left[\left(\tilde{\Psi}, \mathcal{N}[f]\right) \Psi + \left(\tilde{\Psi}^*, \mathcal{N}[f]\right) \Psi^*\right]. \quad (33)$$

These equations can be solved perturbatively for sufficiently small $|A|$, and the right-hand-side of Equation (32) is expanded as

$$\frac{dA}{dt} = \lambda_1 A + c_3 A |A|^2 + c_5 A |A|^4 + c_7 A |A|^6 + \dots, \quad (34)$$

where the eigenvalue λ_1 and the coefficients c_3, c_5, \dots depend on the coupling constant K . Note that the right-hand-side of Equation (34) has only odd order terms. See Appendix Appendix F for the derivations and explicit forms of the coefficients.

The complex amplitude equation Equation (34) can be reduced to a real equation written as

$$\frac{d\sigma}{dt} = 2\sigma G(\sigma), \quad (35)$$

where $\sigma = |A|^2 \geq 0$ and

$$G(\sigma) = \text{Re}(\lambda_1) + \text{Re}(c_3)\sigma + \text{Re}(c_5)\sigma^2 + \text{Re}(c_7)\sigma^3 + \dots. \quad (36)$$

If the asymptotic state in $t \rightarrow \infty$ is stationary, then the right-hand-side of the amplitude equation Equation (35) should be zero. The nonsynchronized state corresponds to the solution $\sigma = 0$, which always satisfies the stationary condition.

The amplitude equation is useful to determine the continuity of the synchronization transition from the nonsynchronized state f^0 to a partially synchronized state. Around the critical point K_c , the order parameter should be small and we can use the truncated equation

$$\text{Re}(\lambda_1) + \text{Re}(c_3)\sigma = 0. \quad (37)$$

Remembering the instability condition $\text{Re}(\lambda_1) > 0$, this equation has a nontrivial solution for $\text{Re}(c_3) < 0$. To the contrary, for $\text{Re}(c_3) > 0$, there is no solution of $\sigma \geq 0$ around the trivial one $\sigma = 0$. We may expect continuity of $c_3(K)$ with respect to K . Thus, taking the limit $K \rightarrow K_c + 0$, we say that the synchronization transition is continuous if $c_3(K_c) < 0$, and is discontinuous if $c_3(K_c) > 0$ [22]. The separating point $\Omega = 1$ on the symmetry line $\gamma_1 = 1$ between the domains A and B is obtained by searching the point which satisfies $\text{Re}(c_3(K_c)) = 0$.

5. Criteria for determining domains

Looking back the five bifurcation diagrams exhibited in Fig. 2, we have two elements to characterize the diagrams, which are oscillation and a jump of the order parameter. We first discuss mechanisms of the oscillation and of the jump in Secs. 5.1 and 5.2 respectively with the aid of the linear and nonlinear analyses reviewed in the previous section 4. After that, we propose a procedure to divide the parameter space into the five domains in Sec. 5.3.

5.1. Oscillation of order parameter

We discuss oscillation of the order parameter by using the fake eigenvalues of the linear operator \mathcal{L} . The order parameter is computed as

$$z(t) = 2\pi \int_{-\infty}^{\infty} \tilde{f}_{-1}(\omega, t) d\omega, \quad (38)$$

hence the time evolution of the order parameter $z(t)$ is described by the eigenvalues arised from the Fourier -1 mode. As defined in the end of Sec. 4.1, the two fake eigenvalues, the roots of $D_{-1}(\lambda)$, are denoted by λ_1^* and λ_2^* , where $\text{Re}(\lambda_1^*) \geq \text{Re}(\lambda_2^*)$.

Let us increase the value of the coupling constant K from the nonsynchronized region $K < K_c$. Beyond the critical point K_c , the first fake eigenvalue λ_1^* becomes unstable and the resonant oscillators, whose natural frequencies are close to $\text{Im}(\lambda_1^*)$, form a cluster. For instance, if $g(\omega)$ is symmetric and unimodal, the resonant frequency is zero and oscillators around $\omega = 0$ form a synchronized cluster. This small cluster corresponds to the continuous synchronization transition in the bifurcation diagram (see Fig. 2 (d)). Further increasing K , for some pairs of (γ_1, Ω) , the second fake eigenvalue λ_2^* also becomes unstable and forms the second cluster. In general the two resonant frequencies differ as $\text{Im}(\lambda_1^*) \neq \text{Im}(\lambda_2^*)$. Thus, the order parameter oscillates due to existence of the two rotating clusters: The order parameter is large when the two clusters are close on \mathbb{S}^1 , and is small when the clusters are in the antiphase positions each other. Summarizing, existence of the two unstable eigenvalues, which mean the two pairs of the unstable eigenvalues by counting the roots of $D_1(\lambda)$ in addition to the roots of $D_{-1}(\lambda)$, suggests the oscillation of the order parameter.

In particular, the symmetry of $g(\omega)$ accepts that the two fake eigenvalues λ_1^* and λ_2^* become unstable at K_c . This simultaneous destabilization yields the bifurcation diagram Fig. 2 (c). However, the symmetry does not always induce the simultaneous destabilization and only one fake eigenvalue gets unstable for $K > K_c$, which yields the bifurcation diagrams Figs. 2 (a) and (b).

To support the mechanism above, we investigate K dependence of the fake eigenvalues λ_1^* and λ_2^* . We choose some points from the domains C, D, and E.

A symmetric case is examined in Fig. 3 for $(\gamma_1, \Omega) = (1, 3)$ which belongs to the domain C. As we expected, two eigenvalues become unstable at the same K_c with different imaginary parts. In Fig. 1 the separating point $\Omega = \sqrt{3}$ between the domains B and C on the symmetry line $\gamma_1 = 1$ is obtained by checking existence of the two unstable eigenvalues.

For the point $(\gamma_1, \Omega) = (0.8, 3)$ belonging to the domain D, the simultaneity of destabilization breaks as shown in Fig. 4 due to asymmetry of $g(\omega)$. The correspondence between the two unstable eigenvalues and the two clusters is exhibited in Fig. 5. The N -body simulation of the Kuramoto model Equation (1) was performed by using the fourth-order Runge-Kutta algorithm with the time step $\Delta t = 0.01$. To

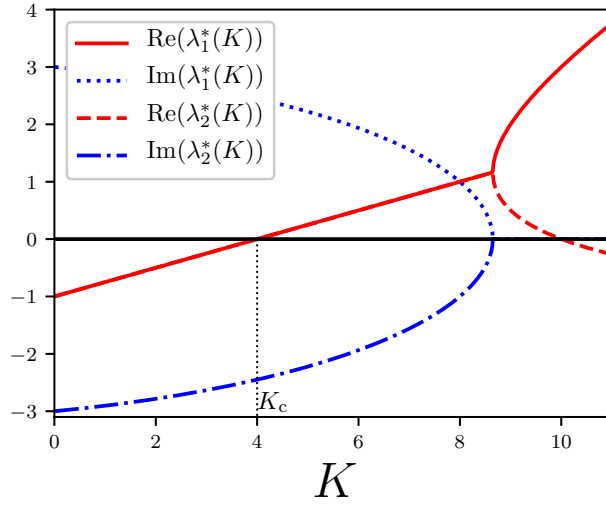


Figure 3. K dependence of the fake eigenvalues λ_1^* and λ_2^* for $(\gamma_1, \Omega) = (1, 3)$. The lines representing $\text{Re}(\lambda_1^*(K))$ (red solid line) and $\text{Re}(\lambda_2^*(K))$ (red dashed line) collapse for $K \leq 4(\sqrt{10} - 1) \simeq 8.649$. The two fake eigenvalues λ_1^* and λ_2^* become unstable simultaneously at $K_c = 4$.

the contrary, at the point $(\gamma_1, \Omega) = (0.9, 1.8)$ belonging to the domain E but close to the domain D, the second fake eigenvalue approaches to zero but does not become unstable as reported in Fig. 6.

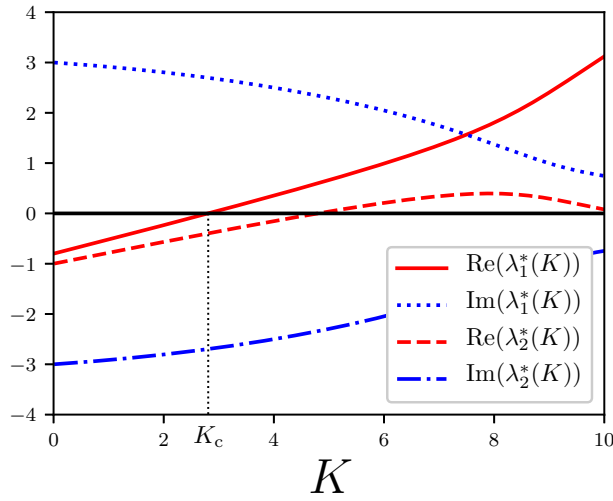


Figure 4. K dependence of the fake eigenvalues λ_1^* and λ_2^* for $(\gamma_1, \Omega) = (0.8, 3)$ belonging to the domain D. The first fake eigenvalue λ_1^* becomes unstable at the critical point $K_c = 2.80796074$, then the second fake eigenvalue λ_2^* becomes unstable at a larger $K = 4.79486605$.

We note that the discussion above does not always hold, because the second unstable eigenvalue does not always yield the second cluster. At the point $(\gamma_1, \Omega) =$

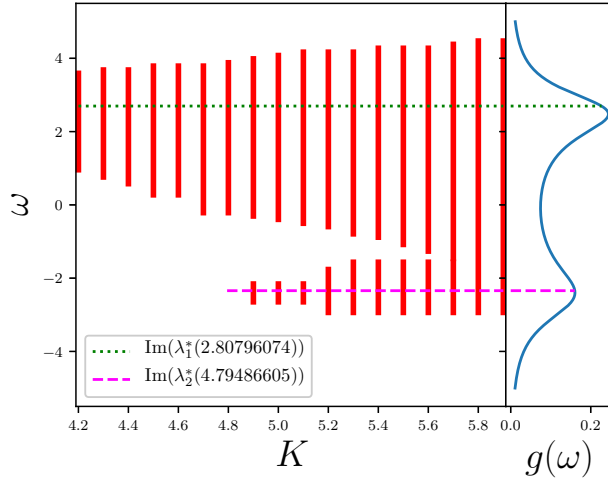


Figure 5. The natural frequency distribution and the emerging clusters. $(\gamma_1, \Omega) = (0.8, 3)$. The clusters, which are obtained by numerically integrating the N -body system Equation (1) with $N = 10^5$, are found in the ranges of red lines. The second fake eigenvalue λ_2^* becomes unstable at $K = 4.79486605$, which corresponds to the emergence point of the second lower cluster.

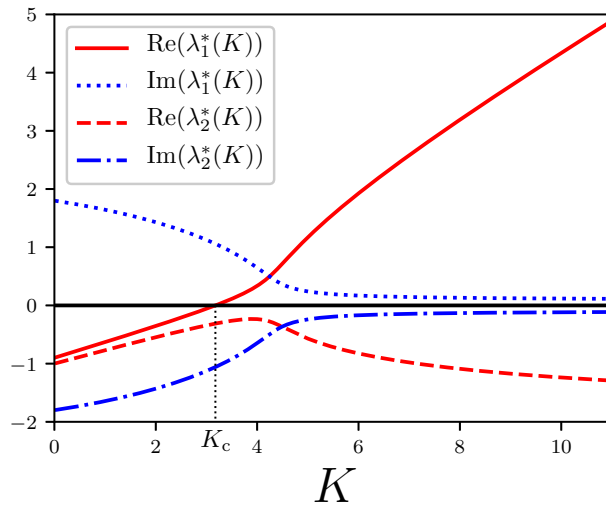


Figure 6. Same with Fig. 4 but for $(\gamma_1, \Omega) = (0.9, 1.8)$ belonging to the domain E. The real part of the fake eigenvalue λ_2 approaches to zero, but does not become positive.

(0.8, 2.6) belonging to the domain E, the second unstable eigenvalue emerges at $K = 5.03248799$, however the imaginary part of the second unstable eigenvalue is not sufficiently far from the grown first cluster and the second virtual cluster is absorbed by the first cluster without emerging as shown in Fig. 7. Therefore, one more condition must be added to characterize the oscillation: $|\text{Im}(\lambda_1^*) - \text{Im}(\lambda_2^*)|$ must be sufficiently large. However, it is not straightforward to determine the threshold for this discrepancy and we leave this condition as a future problem.

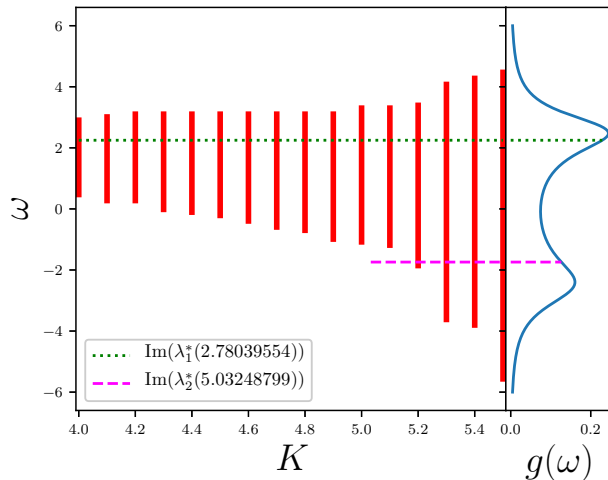


Figure 7. Same with Fig. 5 but for $(\gamma_1, \Omega) = (0.8, 2.6)$ belonging to the domain E. The second fake eigenvalue becomes unstable at $K = 5.03248799$, but the second cluster does not appear.

5.2. Jump of order parameter

Jumps of the order parameter emerge from $r = 0$ (domain B) or from $r > 0$ (domain E). We expect that the jump from $r = 0$ is identified by $\text{Re}(c_3(K_c)) < 0$ as discussed in Sec. 4.2. This criterion is successfully used in a generalized model [22], but for symmetric natural frequency distributions $g(\omega)$. We will verify this criterion for asymmetric $g(\omega)$, that is $\gamma < 1$.

To characterize the jump from $r > 0$, a typical bifurcation diagram of the type E is schematically shown in Fig. 8. This type of jump implies existence of three nontrivial stationary values of r (two stable and one unstable) at $K = K_3 > K_c$, whereas the types A and B have one nontrivial value at most.

These nontrivial values of r correspond to nontrivial roots of $G(\sigma)$ in the amplitude equation Equation (36). To capture the three nontrivial roots of the type E, we consider $G(\sigma)$ up to the third order, which is denoted by $G_3(\sigma)$. Corresponding to the four values of K_i ($i = 1, 2, 3, 4$) in Fig. 8, four schematic graphs of $G_3(\sigma)$ are shown in Fig. 9. Existence of three roots is expressed by the positive discriminant of $G_3(\sigma)$. However, this criterion fails to identify the domain E.

The amplitude equation is derived by using a perturbation technique and a large amplitude is out of range. To ensure the validity of perturbation, we require the

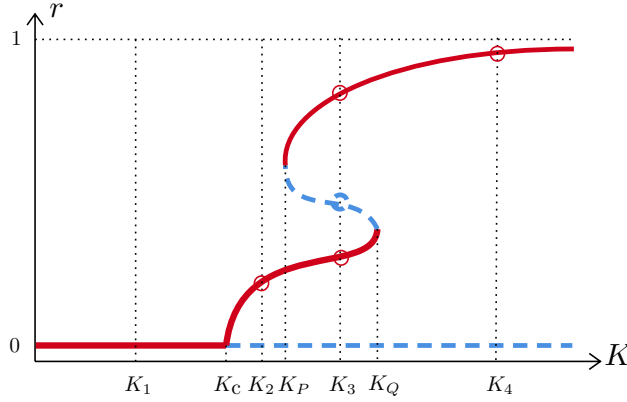


Figure 8. Schematic picture for the bifurcation diagram type E. K_1, K_2, K_3 and K_4 are sample points for capturing the number of roots of $G(\sigma)$ associated with the amplitude equation, as shown in Fig. 9. The red solid lines denote the stable branches, and the blue dashed lines denote the unstable branches.

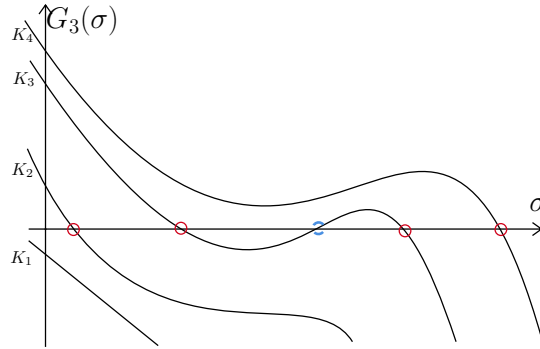


Figure 9. Schematic graphs of $G_3(\sigma)$ for K_1, K_2, K_3 and K_4 , which correspond to those in Fig. 8.

condition

$$|\operatorname{Re}(c_3(K))\sigma| \gg |\operatorname{Re}(c_5(K))\sigma^2| \gg |\operatorname{Re}(c_7(K))\sigma^3|. \quad (39)$$

However, setting σ which corresponds to the value $r(K_Q)$, the condition breaks almost any point on the parameter plane (γ_1, Ω) due to the third order term, while the first and second order terms satisfy

$$|\operatorname{Re}(c_3(K))\sigma| = 2 |\operatorname{Re}(c_5(K))\sigma^2|. \quad (40)$$

See Appendix Appendix G.

We, therefore, change the strategy as follows. At least around the domain B, we may expect that the continuous transition branch, the lower nontrivial stable branch in Fig. 8, should be short and that the bifurcation point at K_Q is close to $r = 0$. This bifurcation point is captured by truncating $G(\sigma)$ up to the second order, denoted by $G_2(\sigma)$. Thus, the new criterion to characterized the domain E is that there exists $K > K_c$ at which the discriminant of $G_2(\sigma)$ is zero.

5.3. Theoretical division of the parameter space

Based on the discussions of Secs. 5.1 and 5.2, we divide the parameter space (γ_1, Ω) into the five domains by the following flow. For preparation, we compute the critical point K_c for a given pair of parameters (γ_1, Ω) as shown in Appendix Appendix D.

We first focus on the critical point $K = K_c$. The discontinuous jump appears at K_c only in the type B among the considered five bifurcation diagrams (see Fig. 2). Therefore, the point (γ_1, Ω) must belong to the domain B if $\text{Re}(c_3(K_c)) > 0$ holds, which suggests a jump from $r = 0$. When this condition does not hold, we check if there are two unstable eigenvalues at K_c . If this condition is satisfied, oscillation of the order parameter starts from K_c and the point (γ_1, Ω) is considered to be in the domain C.

When both checks at K_c are negative, we increase K from K_c and examine the following two propositions:

$$\text{(Oscillation)} \exists K_O (> K_c) \text{ s.t. } \text{Re}(\lambda_2(K_O)) > 0, \quad (41)$$

and

$$\text{(Jump)} \exists K_J (> K_c) \text{ s.t. } \Delta(K_J) = 0, \quad (42)$$

where the discriminant $\Delta(K)$ of $G_2(\sigma)$ is defined by

$$\Delta(K) = \text{Re}(c_3(K))^2 - 4\text{Re}(\lambda(K))\text{Re}(c_5(K)). \quad (43)$$

If both the propositions Equation (41) and Equation (42) are false, we decide that the point (γ_1, Ω) belongs to the domain A. If the oscillation proposition Equation (41) is true but the jump proposition Equation (42) is false, the point must be in the domain D. If the oscillation proposition Equation (41) is false but the jump proposition Equation (42) is true, the point must be in the domain E. If both the propositions are true, then there is a competition between K_O and K_J : $K_O < K_J$ suggests the domain D and $K_O > K_J$ suggests the domain E.

The flow proposed above provides three theoretical lines, I, II, and III which divide the parameter space (γ_1, Ω) into the five domains, as reported in Fig. 10. The theoretical lines reproduce qualitatively the numerically obtained domains.

For the line I, our result is fairly consistent with numerical ones, but the domain D is overestimated. Our method says that the emergence of two clusters is associated with the emergence of two unstable eigenvalues. However, as we discussed previously, the second eigenvalue does not always give rise to the second cluster. We have to reduce the domain D by introducing an additional condition that $|\text{Im}(\lambda_1^*) - \text{Im}(\lambda_2^*)|$ is sufficiently large.

The line II is perfect, because the order parameter is small around the critical point of the synchronization transition, and the perturbatively obtained amplitude equation is valid for such a small amplitude. This criterion has been used for symmetric $g(\omega)$, but we have confirmed that it is also powerful for asymmetric ones. The line II also reveals existence of discontinuous synchronization transition for unimodal but asymmetric distributions. The existence has been pointed out numerically in a previous study [25], but our theoretical analysis ensures it.

The line III is not perfect but captures the domain E qualitatively. As we expected, the theoretical prediction becomes precise around the domain B. We, therefore, conclude that the higher order analysis of the amplitude equation is useful to predict the type of a bifurcation diagram.

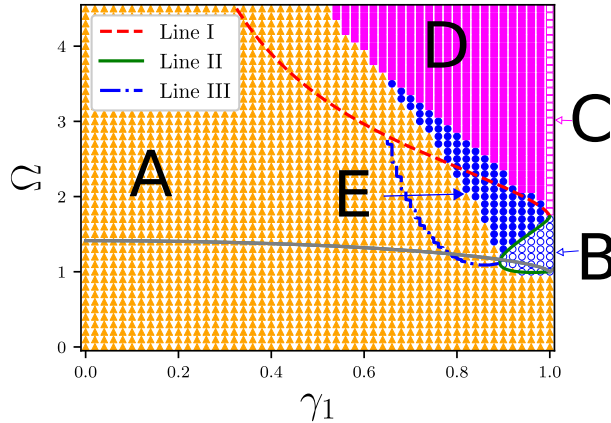


Figure 10. Theoretical classification of the parameter space. The domain B is perfectly enclosed by the line I. The theoretical domain E is enclosed by the lines II and III.

6. Conclusion and Discussions

We have proposed a theoretical method to classify bifurcation diagrams in the Kuramoto model by using the amplitude equation with the aid of the linear analysis around the nonsynchronized reference state. The amplitude equation, obtained perturbatively, is usually stopped up to the second leading term, since it is sufficient to judge the continuity of the synchronization transition. However, introducing asymmetry into the natural frequency distribution, new types of bifurcation diagrams appear and the second leading term is not sufficient to characterize them. We have extended the amplitude equation up to the third leading term and successfully captured a discontinuous bifurcation after a continuous one.

For the bifurcation diagrams having oscillatory states, we focused on the unstable eigenvalues of the nonsynchronized state. Roughly speaking, one unstable eigenvalue corresponds to one cluster formation, and hence existence of two unstable eigenvalues suggest appearance of two clusters rotating with different speeds. This idea is qualitatively in good agreement with numerical results, but overestimates the domain having the oscillation. We have to reduce the domain by adding one more condition which requires a large discrepancy of rotating speeds of the two clusters in order to avoid the absorption of the second virtual cluster by the first grown cluster. Introducing the additional condition has to be done. We remark that a similar condition was discussed in a Hamiltonian system [28].

Finally, we discuss on applications of our theory to general coupled oscillator models. Introducing the phase-lag parameter in the coupling function [29], we have a phase diagram having a continuous synchronization transition followed by a discontinuous jump as the type E [30]. Analyzing this system is a straightforward application of our theory. Studying time delay [31, 32] is also an interesting application. If the coupling function becomes general, the coefficients of the amplitude equation may have divergences as the coupling constant goes to the critical value [21]. For instance, the coefficient $\text{Re}(c_3)$ may be proportional to $1/\text{Re}(\lambda_1)$. It is another future problem to study whether the proposed criterion is persistent under

such divergences of coefficients.

Acknowledgments

Y.Y.Y. acknowledges the support of JSPS KAKENHI Grant No. 16K05472.

Appendix A. Ott-Antonsen ansatz and reduction

The Ott-Antonsen ansatz assumes the form of the probability distribution $F(\theta, \omega, t)$ as

$$F = \frac{g(\omega)}{2\pi} \left\{ 1 + \sum_{k=1}^{\infty} [a(\omega, t)^k e^{ik\theta} + a^*(\omega, t)^k e^{-ik\theta}] \right\} \quad (\text{A.1})$$

where $|a(\omega, t)| < 1$ is assumed to ensure the convergence of the series. By substituting (A.1) to (8), we have

$$\frac{\partial a}{\partial t} + i\omega t + \frac{K}{2} (a^2 z - z^*) = 0, \quad (\text{A.2})$$

where the order parameter is written as

$$z = \int_{-\infty}^{\infty} g(\omega) a^*(\omega, t) d\omega. \quad (\text{A.3})$$

Since $|g(\omega) a^*(\omega, t)| < g(\omega)$ holds and $g(\omega)$ decays faster than $1/|\omega|$ when $|\omega| \rightarrow \infty$, the integration of (A.3) can be computed by using the residue theorem as

$$z(t) = k_1 a^*(\Omega + i\gamma_1, t) + k_2 a^*(-\Omega + i\gamma_2, t), \quad (\text{A.4})$$

where the constants k_1 and k_2 are defined by Equation (13). Introducing the complex variables z_1 and z_2 as

$$z_1 = a^*(\Omega + i\gamma_1, t), \quad z_2 = a^*(-\Omega + i\gamma_2, t), \quad (\text{A.5})$$

the order parameter is expressed as

$$z = k_1 z_1 + k_2 z_2. \quad (\text{A.6})$$

Setting $\omega = \Omega + i\gamma_1$ and $\omega = -\Omega + i\gamma_2$ in Equation (A.2), dynamics of z_1 and z_2 are described by the equation Equation (12).

Appendix B. Spectral functions and eigenfunctions

The linear operator \mathcal{L} is expanded into the Fourier series as

$$\mathcal{L}f = \sum_{k \in \mathbb{Z}} \mathcal{L}_k \tilde{f}_k(\omega, t) e^{ik\theta}, \quad (\text{B.1})$$

where \tilde{f}_k are the Fourier components of f defined by Equation (21). The linear operator \mathcal{L}_k is defined by

$$\mathcal{L}_k \tilde{f}_k = -ik\omega \tilde{f}_k + \frac{K}{2} g(\omega) (\delta_{k,1} + \delta_{k,-1}) \int_{-\infty}^{\infty} \tilde{f}_k(\omega, t) d\omega. \quad (\text{B.2})$$

The symbol $\delta_{k,l}$ represents the Kronecker delta.

Let $\psi(\omega)$ be an eigenfunction of the linear operator \mathcal{L}_k associated with the eigenvalue λ , that is,

$$\mathcal{L}_k \psi = \lambda \psi. \quad (\text{B.3})$$

Then, we can confirm that

$$\Psi(\theta, \omega) = \psi(\omega)e^{ik\theta} \quad (\text{B.4})$$

is an eigenfunction of the linear operator \mathcal{L} as

$$\mathcal{L}(\psi e^{ik\theta}) = \lambda(\psi e^{ik\theta}). \quad (\text{B.5})$$

We, therefore, discuss the eigenvalues of the Fourier expanded linear operators \mathcal{L}_k . The modes $k \neq \pm 1$ have $\mathcal{L}_k = -ik\omega$ and have solely rotations. Hereafter, we focus on the modes $k = \pm 1$.

Using the explicit form of \mathcal{L}_k Equation (B.2), the equation Equation (B.3) is rewritten as

$$(\lambda + ik\omega)\psi(\omega) = \frac{K}{2}g(\omega) \int_{-\infty}^{\infty} \psi(\omega')d\omega'. \quad (\text{B.6})$$

Let $\lambda + ik\omega \neq 0$. Multiplying $(\lambda + ik\omega)^{-1}$ and integrating over ω , we have

$$\left(\int_{-\infty}^{\infty} \psi(\omega)d\omega \right) \Lambda_k(\lambda) = 0, \quad (\text{B.7})$$

where the spectral functions $\Lambda_{\pm 1}(\omega)$ are defined in Equation (22). If $\int_{-\infty}^{\infty} \psi(\omega)d\omega = 0$, then $\psi(\omega) \equiv 0$ for any $\omega \in \mathbb{R}$ from Equation (B.6) and the assumption $\lambda + ik\omega \neq 0$, but this is not compatible with the assumption that ψ is the eigenfunction. Consequently, the eigenvalue λ must satisfy the equation $\Lambda_k(\lambda) = 0$. Assuming the integral $\int_{-\infty}^{\infty} \psi(\omega)d\omega = 1$ without loss of generality, the eigenfunction ψ can be expressed as

$$\psi(\omega) = \frac{K}{2} \frac{g(\omega)}{\lambda + ik\omega}, \quad (k = \pm 1). \quad (\text{B.8})$$

Appendix C. Analytic continuation

We introduce the analytic continuation of the spectral functions $\Lambda_{\pm 1}(\lambda)$, Equation (22). We start from a point λ whose real part is positive, $\text{Re}(\lambda) > 0$, then decrease the real part. The starting point, $\text{Re}(\lambda) > 0$, comes from the Laplace transform [27]

$$\hat{f}(s) = \int_0^{\infty} f(t)e^{-st}dt, \quad (\text{C.1})$$

which analyzes temporal evolution and is defined in the positive real half-plane $\text{Re}(s) > 0$ to ensure convergence of the integral. The variable s corresponds to λ .

When λ passes the imaginary axis, the integrands of the spectral functions $\Lambda_{\pm 1}(\lambda)$, Equation (22), meet the singularities at $\omega = \pm i\lambda$. To avoid this singularity at $\omega = i\lambda$ ($\omega = -i\lambda$), we modify continuously the integral contour from the real axis by adding a small lower (upper) half-circle around the singular point. This modification brings a residue part to the integral. Continuing this modification for $\text{Re}(\lambda) < 0$, we have analytically continued functions of $\Lambda_{\pm 1}(\lambda)$ as

$$D_{\pm 1}(\lambda) = 1 - \frac{K}{2}I_{\pm 1}(\lambda), \quad (\text{C.2})$$

where

$$I_{\pm 1}(\lambda) = \begin{cases} \int_{-\infty}^{\infty} \frac{g(\omega)}{\lambda \pm i\omega} d\omega, & \text{Re}(\lambda) > 0 \\ \text{PV} \int_{-\infty}^{\infty} \frac{g(\omega)}{\lambda \pm i\omega} d\omega + \pi g(\pm i\lambda), & \text{Re}(\lambda) = 0 \\ \int_{-\infty}^{\infty} \frac{g(\omega)}{\lambda \pm i\omega} d\omega + 2\pi g(\pm i\lambda), & \text{Re}(\lambda) < 0 \end{cases} \quad (\text{C.3})$$

and PV represents the Cauchy principal value. The roots of $D_{\pm 1}(\lambda)$ and of $\Lambda_{\pm 1}(\lambda)$ are identical from their definitions if $\text{Re}(\lambda) > 0$. However, they do not coincide in general for $\text{Re}(\lambda) \leq 0$. Therefore, a root of $D_{\pm 1}(\lambda)$ with $\text{Re}(\lambda) \leq 0$ is not an eigenvalue but is called a resonance pole, a Landau pole, or a fake eigenvalue [33].

The difference between $\Lambda_1(\lambda)$ and $D_1(\lambda)$ is demonstrated by considering a Lorentzian natural frequency distribution,

$$g(\omega) = \frac{\gamma}{\pi} \frac{1}{\omega^2 + \gamma^2}. \quad (\text{C.4})$$

Straightforward computations give

$$\Lambda_1(\lambda) = \begin{cases} 1 - \frac{K}{2(\lambda + \gamma)}, & \text{Re}(\lambda) > 0 \\ 1 - \frac{K}{2(\lambda - \gamma)}, & \text{Re}(\lambda) < 0 \end{cases} \quad (\text{C.5})$$

and

$$D_1(\lambda) = 1 - \frac{K}{2(\lambda + \gamma)}, \quad \lambda \in \mathbb{C}. \quad (\text{C.6})$$

Therefore, $\lambda = K/2 - \gamma$ is a root of $D_1(\lambda)$ but is not of $\Lambda_1(\lambda)$ if $K \leq K_c$ and $\text{Re}(\lambda) \leq 0$ accordingly, where $K_c = 2\gamma$ is the synchronization transition point. Similarly, we can reproduce the critical point $K_c = 2/[\pi g(0)]$ for a symmetric unimodal $g(\omega)$ by computing the roots of $D_{\pm 1}(\lambda)$. The critical point K_c for the considering family Equation (2) is given in Appendix Appendix D.

Appendix D. Fake eigenvalues and synchronization transition point K_c

Appendix D.1. Fake eigenvalues

Substituting Equation (2) to Equation (C.3), we obtain the explicit form of $D_1(\lambda)$ as

$$D_1(\lambda) = 1 - \frac{K}{2\gamma^+} \frac{\gamma^+ \lambda + (\gamma^+)^2 + i\Omega\gamma^-}{(\lambda + \gamma_1 + i\Omega)(\lambda + \gamma_2 - i\Omega)} \quad (\text{D.1})$$

where

$$\gamma^+ = \gamma_1 + \gamma_2 > 0, \quad \gamma^- = \gamma_1 - \gamma_2 \leq 0. \quad (\text{D.2})$$

The equation $D_1(\lambda) = 0$ induces the quadratic equation

$$\lambda^2 - b(K)\lambda - a_R(K) - ia_I(K) = 0 \quad (\text{D.3})$$

where

$$b(K) = \frac{K}{2} - \gamma^+, \quad (\text{D.4})$$

$$a_R(K) = \frac{K}{2}\gamma^+ - (\gamma_1\gamma_2 + \Omega^2), \quad (\text{D.5})$$

$$a_I(K) = \Omega\gamma^- \left(1 + \frac{K}{2\gamma^+}\right) \leq 0. \quad (\text{D.6})$$

To write down the two solutions to Equation (D.3), we introduce the complex variable

$$x = b^2 + 4a_R + i4a_I = \rho e^{i\theta}, \quad \rho, \theta \in \mathbb{R}. \quad (\text{D.7})$$

The argument θ is in the interval $[\pi, 2\pi]$ from $a_I \leq 0$. The two fake eigenvalues λ_1 and λ_2 , which satisfy $\text{Re}(\lambda_1) \geq \text{Re}(\lambda_2)$, are written as

$$2\lambda_1 = b - \sqrt{\rho} \cos \frac{\theta}{2} - i\sqrt{\rho} \sin \frac{\theta}{2}, \quad (\text{D.8})$$

$$2\lambda_2 = b + \sqrt{\rho} \cos \frac{\theta}{2} + i\sqrt{\rho} \sin \frac{\theta}{2}, \quad (\text{D.9})$$

$$(\text{D.10})$$

as $\cos(\theta/2) \leq 0$. Note that the signs of the imaginary parts are $\text{Im}(\lambda_1) \leq 0$ and $\text{Im}(\lambda_2) \geq 0$ from $\sin(\theta/2) \geq 0$ and that they are consistent with Figs. 3-7.

The synchronization transition point K_c is determined by the equation $\text{Re}(\lambda_1(K_c)) = 0$. Let us show that the solution is at most one. Using the relation

$$\cos \frac{\theta}{2} = -\sqrt{\frac{1 + \cos \theta}{2}} \quad (\text{D.11})$$

and the definitions of ρ and θ ,

$$\rho = \sqrt{(b^2 + 4a_R)^2 + (4a_I)^2}, \quad \cos \theta = \frac{b^2 + 4a_R}{\rho}, \quad (\text{D.12})$$

we have

$$2\text{Re}(\lambda_1(K)) = b + \frac{1}{\sqrt{2}} \sqrt{\sqrt{(b^2 + 4a_R)^2 + (4a_I)^2} + b^2 + 4a_R}. \quad (\text{D.13})$$

The functions $b(K)$, $a_I^2(K)$, and $b^2(K) + 4a_R(K)$ are increasing functions of K for $K > 0$, since

$$b^2 + 4a_R = \left(\frac{K}{2} + \gamma^+\right)^2 - 4(\gamma_1\gamma_2 + \Omega^2). \quad (\text{D.14})$$

Therefore, the real part $\text{Re}(\lambda_1(K))$ is also an increasing function of K for $K > 0$ and takes zero at most once time.

Appendix D.2. Synchronization transition point K_c

We show that there exists the unique solution to the equation $\text{Re}(\lambda_1(K)) = 0$, which determines the synchronization transition point K_c . At K_c , the fake eigenvalue λ must be pure imaginary of the form $\lambda = i\lambda_I$ ($\lambda_I \in \mathbb{R}$). Substituting this form with $K = K_c$ into the quadratic equation Equation (D.3), we have

$$-\lambda_I^2 - ib(K_c)\lambda_I - a_R(K_c) - ia_I(K_c) = 0. \quad (\text{D.15})$$

The real part reads

$$\lambda_I^2 + a_R(K_c) = 0 \quad (\text{D.16})$$

and the imaginary part reads

$$b(K_c)\lambda_I + a_I(K_c) = 0. \quad (\text{D.17})$$

Eliminating λ_I from Equation (D.16) and Equation (D.17), we have the cubic equation to determine K_c as

$$\begin{aligned} & (\gamma^+)^3 K_c^3 - 2 \{2(\gamma^+)^4 + \gamma_1\gamma_2 [(\gamma^+)^2 + 4\Omega^2]\} K_c^2 \\ & + 4\gamma^+ [(\gamma^+)^4 + 2\gamma_1\gamma_2(\gamma^+)^2 + 4\Omega^2 (\gamma_1^2 + \gamma_2^2)] K_c \\ & - 8\gamma_1\gamma_2(\gamma^+)^2 [(\gamma^+)^2 + 4\Omega^2] = 0. \end{aligned} \quad (\text{D.18})$$

All the real solutions are positive because the left-hand-side of Equation (D.18) is always negative for $K_c < 0$. The number of real solutions to Equation (D.18) is one or three, and the synchronization transition point is determined as the smallest real solution to Equation (D.18).

In order to investigate the number of unstable eigenvalues, we introduce the discriminant Δ_3 for the cubic equation Equation (D.18). In general, the discriminant is defined as

$$\Delta_3 = b^2c^2 - 27a^2d^2 - 4ac^3 - 4b^3d + 18abcd \quad (\text{D.19})$$

for the cubic equation

$$ax^3 + bx^2 + cx + d = 0. \quad (\text{D.20})$$

The number of real solutions is one for $\Delta_3 < 0$ and is three for $\Delta_3 > 0$.

In the case $\Delta_3 < 0$ the first fake eigenvalue λ_1 passes the imaginary axis at the unique real solution K_c and no other passing occurs. In the case $\Delta_3 > 0$ we have three different real solutions of $K_c^{(1)}$, $K_c^{(2)}$, and $K_c^{(3)}$, where $K_c^{(1)} < K_c^{(2)} < K_c^{(3)}$. By the definition, the first fake eigenvalue λ_1 passes the imaginary axis at $K_c = K_c^{(1)}$ and it does not pass the imaginary axis any more as shown in the previous subsection Appendix D.1. As a consequence, the other two solutions $K_c^{(2)}$ and $K_c^{(3)}$ are realized by the second fake eigenvalue λ_2 : It passes the imaginary axis from left to right at $K_c^{(2)}$, and from right to left at $K_c^{(3)}$, as observed in Fig. 4.

Appendix E. Adjoint linear operator

The adjoint operator \mathcal{L}^\dagger acts on f as

$$\mathcal{L}^\dagger f = \omega \frac{\partial f}{\partial \theta} + \frac{K}{2} (r_1 [f f^0] e^{-i\theta} + r_{-1} [f f^0] e^{i\theta}), \quad (\text{E.1})$$

where

$$r_n[f] = \int_{-\infty}^{\infty} d\omega \int_{-\pi}^{\pi} d\theta f(\theta, \omega, t) e^{in\theta}. \quad (\text{E.2})$$

As done for the linear operator \mathcal{L} , we expand \mathcal{L}^\dagger into the Fourier series as

$$\mathcal{L}^\dagger f = \sum_{k \in \mathbb{Z}} \mathcal{L}_k^\dagger \tilde{f}_k(\omega, t) e^{ik\theta}. \quad (\text{E.3})$$

The linear operator \mathcal{L}_k^\dagger is defined by

$$\mathcal{L}_k^\dagger \tilde{f}_k = ik\omega \tilde{f}_k + \frac{K}{2} [\delta_{k,1} + \delta_{k,-1}] \int_{-\infty}^{\infty} \tilde{f}_k(\omega, t) g(\omega) d\omega \quad (\text{E.4})$$

We focus on the modes $k = \pm 1$.

Let μ be an eigenvalue of \mathcal{L}_k^\dagger and $\tilde{\psi}(\omega)$ be the corresponding eigenfunction which satisfy

$$\mathcal{L}_k^\dagger \tilde{\psi} = \mu \tilde{\psi}. \quad (\text{E.5})$$

This equation brings

$$(\mu - ik\omega) \tilde{\psi}(\omega) = \frac{K}{2} \int_{-\infty}^{\infty} \tilde{\psi}(\omega) g(\omega) d\omega. \quad (\text{E.6})$$

Repeating the same discussion done in Appendix Appendix B, the eigenvalue μ must satisfy

$$\tilde{\Lambda}_k^*(\mu^*) = 0. \quad (\text{E.7})$$

This equation implies that λ^* is an eigenvalue of \mathcal{L}_k^\dagger if λ is an eigenvalue of \mathcal{L}_k .

Let λ be an eigenvalue of \mathcal{L}_1 and ψ be the corresponding eigenfunction Equation (B.8). Then, \mathcal{L}_1^\dagger has an eigenvalue λ^* and the corresponding eigenfunction is computed as

$$\tilde{\psi}(\omega) = \frac{1}{[\Lambda'(\lambda)]^*} \frac{1}{\lambda^* - i\omega}. \quad (\text{E.8})$$

Thus, λ^* is also an eigenvalue of \mathcal{L}^\dagger and the corresponding eigenfunction is

$$\tilde{\Psi}(\theta, \omega) = \frac{\tilde{\psi}(\omega)}{2\pi} e^{i\theta}, \quad (\text{E.9})$$

which satisfies the normalization condition

$$\left(\tilde{\Psi}, \Psi \right) = 1. \quad (\text{E.10})$$

Appendix F. Derivation of the amplitude equation

Appendix F.1. Derivations of equations for A and H

We assume that λ is the unique unstable eigenvalue of \mathcal{L}_1 and $\psi(\omega)$ is the corresponding eigenfunction. The relation $\Lambda_{-1}(\lambda^*) = \Lambda_1^*(\lambda)$ implies that λ^* is an eigenvalue of \mathcal{L}_{-1} and $\psi^*(\omega)$ is the corresponding eigenfunction. Therefore, the linear operator \mathcal{L} has two unstable eigenvalues λ and λ^* , and the corresponding eigenfunctions respectively

$$\Psi(\theta, \omega) = \psi(\omega) e^{i\theta}, \quad \Psi^*(\theta, \omega) = \psi^*(\omega) e^{-i\theta}. \quad (\text{F.1})$$

Using these eigenfunctions, we expand the perturbation f into the form of Equation (25),

$$f = A(t)\Psi + A^*(t)\Psi^* + H(\theta, \omega, A, A^*). \quad (\text{F.2})$$

We assume that the unstable manifold H is tangent to the unstable eigenspace $\text{Span}(\Psi, \Psi^*)$. Substituting this expansion into the equation of continuity, we have

$$\frac{dA}{dt}\Psi + \frac{dA^*}{dt}\Psi^* + \frac{dH}{dt} = \lambda A\Psi + \lambda^* A^*\Psi^* + \mathcal{L}H + \mathcal{N}[f]. \quad (\text{F.3})$$

In Equation (F.3), taking the inner product with $\tilde{\Psi}$, we obtain the equation for A as

$$\frac{dA}{dt} = \lambda A + \left(\tilde{\Psi}, \mathcal{N}[f] \right). \quad (\text{F.4})$$

Extracting this equality and its complex conjugate from Equation (F.3), we have the equation for H as

$$\frac{dH}{dt} = \mathcal{L}H + \mathcal{N}[f] - \left[\left(\tilde{\Psi}, \mathcal{N}[f] \right) \Psi + \left(\tilde{\Psi}^*, \mathcal{N}[f] \right) \Psi^* \right]. \quad (\text{F.5})$$

The left-hand-side of Equation (F.5) is read as

$$\frac{dH}{dt} = \frac{\partial H}{\partial A} \frac{dA}{dt} + \frac{\partial H}{\partial A^*} \frac{dA^*}{dt}. \quad (\text{F.6})$$

The right-hand-side of Equation (F.4) starts from the linear term λA , while one of Equation (F.5) starts from the quadratic terms of A and A^* by the tangency assumption of the unstable manifold, $H = O(|A|^2)$. We, therefore, solve the two equations Equation (F.4) and Equation (F.5) perturbatively by assuming that $|A|$ is small.

Appendix F.2. Fourier series expansion of H

Before going to the Taylor series expansion with respect to $|A|$, we expand H into the Fourier series as

$$H = \sum_{n \in \mathbb{Z}} H_n(\omega, A, A^*) e^{in\theta}. \quad (\text{F.7})$$

The rotational symmetry of the system yields [20] yields

$$H_n(\omega, A, A^*) = \begin{cases} 0 & n = 0 \\ A\sigma h_1(\sigma, \omega) & n = 1 \\ A^n h_n(\sigma, \omega) & n \geq 2, \end{cases} \quad (\text{F.8})$$

where $\sigma = |A|^2$.

Now we expand h_n into the Taylor series. For sufficiently small σ we expand

$$h_n(\sigma, \omega) = h_{n,0}(\omega) + \sigma h_{n,1}(\omega) + \dots \quad (\text{F.9})$$

Algebraic computations gives the equation of A as

$$\frac{dA}{dt} = \lambda A + c_3 A \sigma + c_5 A \sigma^2 + c_7 A \sigma^3 + \dots \quad (\text{F.10})$$

where

$$c_3 = -\pi K \langle \tilde{\psi}, h_{2,0} \rangle, \quad (\text{F.11})$$

$$c_5 = -\pi K \left[\langle \tilde{\psi}, h_{2,0} \rangle \left(\int h_{1,0} d\omega \right)^* + \langle \tilde{\psi}, h_{2,1} \rangle \right], \quad (\text{F.12})$$

$$c_7 = -\pi K \left[\left(\int h_{1,1} d\omega \right)^* \langle \tilde{\psi}, h_{2,0} \rangle + \langle \tilde{\psi}, h_{2,2} \rangle + \left(\int h_{1,0} d\omega \right)^* \langle \tilde{\psi}, h_{2,1} \rangle \right], \quad (\text{F.13})$$

and

$$\langle f_1, f_2 \rangle = \int_{-\infty}^{\infty} f_1^* f_2 d\omega. \quad (\text{F.14})$$

We compute $\langle \tilde{\psi}, h_{2,0} \rangle$, $\int h_{1,0} d\omega$, $\langle \tilde{\psi}, h_{2,1} \rangle$, $\int h_{1,1} d\omega$, and $\langle \tilde{\psi}, h_{2,2} \rangle$ by expanding Equation (F.5) into the Fourier series. Four Fourier modes are enough to compute c_3 , c_5 , and c_7 .

Appendix F.3. Fourier series expansion of Equation (F.5)

Appendix F.3.1. The first Fourier component H_1 The first Fourier mode gives

$$\frac{dH_1}{dt} = \mathcal{L}_1 H_1 + (\mathcal{N}[f])_1 - \langle \tilde{\psi}, (\mathcal{N}[f])_1 \rangle \psi, \quad (\text{F.15})$$

where $(\mathcal{N}[f])_n$ represents the n th Fourier mode of $\mathcal{N}[f]$. Substituting the Taylor series expansion Equation (F.9), we have the expanded left-hand-side as

$$(2\lambda + \lambda^*) h_{1,0} A \sigma + \{(2c_3 + c_3^*) h_{1,0} + (3\lambda + 2\lambda^*) h_{1,1}\} A \sigma^2 + O(|A|^7) \quad (\text{F.16})$$

and the expanded right-hand-side as

$$\begin{aligned} & A \sigma \left(-i\omega h_{1,0} + \frac{K}{2} g(\omega) \int h_{1,0} d\omega \right) + A \sigma^2 \left(-i\omega h_{1,1} + \frac{K}{2} g(\omega) \int h_{1,1} d\omega \right) \\ & + A \sigma (-\pi K h_{2,0}) + A \sigma^2 \left\{ -\pi K \left(\left(\int h_{1,0} d\omega \right)^* h_{2,0} + h_{2,1} \right) \right\} \\ & - c_3 \psi A \sigma - c_5 \psi A \sigma^2 + O(|A|^7). \end{aligned} \quad (\text{F.17})$$

Comparing the coefficients of $A\sigma$ and $A\sigma^2$, we obtain

$$(2\lambda + \lambda^* + i\omega)h_{1,0} = \frac{K}{2}g(\omega) \int h_{1,0}d\omega - \pi Kh_{2,0} - c_3\psi, \quad (\text{F.18})$$

$$(3\lambda + 2\lambda^* + i\omega)h_{1,1} = \frac{K}{2}g(\omega) \int h_{1,1}d\omega - \pi K \left[\left(\int h_{1,0}d\omega \right)^* h_{2,0} + h_{2,1} \right] - (2c_3 + c_3^*)h_{1,0} - c_5\psi. \quad (\text{F.19})$$

Appendix F.3.2. The second Fourier component H_2 The second Fourier mode gives

$$\frac{dH_2}{dt} = \mathcal{L}_2 H_2 + (\mathcal{N}[f])_2. \quad (\text{F.20})$$

Performing similar calculations above, we obtain

$$h_{2,0} = \frac{\pi K^2}{2} \frac{g(\omega)}{(\lambda + i\omega)^2}, \quad (\text{F.21})$$

$$(3\lambda + \lambda^* + 2i\omega)h_{2,1} = -2c_3 h_{2,0} + 2\pi K \left(\psi \int h_{1,0}d\omega + h_{1,0} - h_{3,0} \right), \quad (\text{F.22})$$

$$2(2\lambda + \lambda^* + i\omega)h_{2,2} = -(3c_3 + c_3^*)h_{2,1} - 2c_5 h_{2,0} + 2\pi K \left[\psi \int h_{1,1}d\omega + h_{1,1} + h_{1,0} \int h_{1,0}d\omega - h_{3,1} - h_{3,0} \left(\int h_{1,0}d\omega \right)^* \right]. \quad (\text{F.23})$$

Appendix F.3.3. The third Fourier component H_3 The third Fourier mode gives

$$\frac{dH_3}{dt} = \mathcal{L}_3 H_3 + (\mathcal{N}[f])_3. \quad (\text{F.24})$$

As above, we obtain

$$h_{3,0} = \frac{\pi^2 K^3}{2} \frac{g(\omega)}{(\lambda + i\omega)^3}, \quad (\text{F.25})$$

$$(4\lambda + \lambda^* + 3i\omega)h_{3,1} = -3c_3 h_{3,0} + 3\pi K \left(h_{2,0} \int h_{1,0}d\omega + h_{2,1} - h_{4,0} \right). \quad (\text{F.26})$$

Appendix F.3.4. The fourth Fourier component H_4 The fourth Fourier mode gives

$$\frac{dH_4}{dt} = \mathcal{L}_4 H_4 + (\mathcal{N}[f])_4. \quad (\text{F.27})$$

As above, we obtain

$$h_{4,0} = \frac{\pi^3 K^4}{2} \frac{g(\omega)}{(\lambda + i\omega)^4}. \quad (\text{F.28})$$

Appendix F.3.5. Integrals and the spectral function Before going to the calculations of c_3 , c_5 , and c_7 , we arrange simple forms of the integrals as

$$\int \frac{g(\omega)}{\lambda + i\omega} d\omega = \frac{2}{K} (1 - \Lambda(\lambda)), \quad (\text{F.29})$$

$$\int \frac{g(\omega)}{(\lambda + i\omega)^2} d\omega = \frac{2}{K} \Lambda'(\lambda), \quad (\text{F.30})$$

$$\int \frac{g(\omega)}{(\lambda + i\omega)^3} d\omega = -\frac{1}{K} \Lambda''(\lambda), \quad (\text{F.31})$$

$$\int \frac{g(\omega)}{(\lambda + i\omega)^4} d\omega = \frac{1}{3K} \Lambda'''(\lambda), \quad (\text{F.32})$$

$$\int \frac{g(\omega)}{(\lambda + i\omega)^5} d\omega = -\frac{1}{12K} \Lambda''''(\lambda), \quad (\text{F.33})$$

where $\Lambda(\lambda)$ represents $\Lambda_1(\lambda)$ and we omitted the subscript for a simple notation. We remark that, in the amplitude equation, we focus on the eigenvalue having positive real part and $\Lambda_1(\lambda) = D_1(\lambda)$ accordingly. The derivations are straightforward by using the definition of the spectral function Equation (22). Now we can compute the coefficients of the amplitude equation, c_3 , c_5 , and c_7 .

Appendix F.4. Calculation of c_3

For c_3 , we calculate $\langle \tilde{\psi}, h_{2,0} \rangle$. From Equation (F.21),

$$\langle \tilde{\psi}, h_{2,0} \rangle = \frac{\pi K^2}{2} \frac{1}{\Lambda'(\lambda)} \int \frac{g(\omega)}{(\lambda + i\omega)^3} d\omega = -\frac{\pi K}{2} \frac{\Lambda''(\lambda)}{\Lambda'(\lambda)}, \quad (\text{F.34})$$

therefore,

$$c_3(K) = \frac{\pi^2 K^2}{2} \frac{\Lambda''(\lambda)}{\Lambda'(\lambda)}. \quad (\text{F.35})$$

Appendix F.5. Calculation of c_5

For c_5 , we calculate $\int h_{1,0} d\omega$ and $\langle \tilde{\psi}, h_{2,1} \rangle$.

Appendix F.5.1. $\int h_{1,0} d\omega$ From Equation (F.18),

$$h_{1,0} = \frac{K}{2} \frac{g(\omega)}{2\lambda + \lambda^* + i\omega} \int h_{1,0} d\omega - \pi K \frac{h_{2,0}}{2\lambda + \lambda^* + i\omega} - c_3 \frac{\psi}{2\lambda + \lambda^* + i\omega}. \quad (\text{F.36})$$

Integrating over ω , we have

$$\Lambda(2\lambda + \lambda^*) \int h_{1,0} d\omega = -\pi K \int \frac{h_{2,0}}{2\lambda + \lambda^* + i\omega} d\omega - c_3 \int \frac{\psi}{2\lambda + \lambda^* + i\omega} d\omega \quad (\text{F.37})$$

$$= -\frac{(\pi K)^2}{2} \left[\frac{1}{\lambda_{\text{R}}} \Lambda'(\lambda) - \frac{1}{2\lambda_{\text{R}}^2} \Lambda(2\lambda + \lambda^*) \right] - \frac{c_3}{2\lambda_{\text{R}}} \Lambda(2\lambda + \lambda^*). \quad (\text{F.38})$$

from Equation (F.21) and Equation (B.8). The symbol λ_{R} represents the real part of the eigenvalue λ .

Appendix F.5.2. $\langle \tilde{\psi}, h_{2,1} \rangle$ From Eq. Equation (F.22) and Eq. Equation (F.25),

$$\begin{aligned} h_{2,1} = & -2c_3 \frac{h_{2,0}}{3\lambda + \lambda^* + 2i\omega} + 2\pi K \left(\int h_{1,0} d\omega \right) \frac{\psi}{3\lambda + \lambda^* + 2i\omega} \\ & + 2\pi K \frac{h_{1,0}}{3\lambda + \lambda^* + 2i\omega} - 2\pi K \frac{h_{3,0}}{3\lambda + \lambda^* + 2i\omega}. \end{aligned} \quad (\text{F.39})$$

Hence, $\langle \tilde{\psi}, h_{2,1} \rangle$ is

$$\begin{aligned} \langle \tilde{\psi}, h_{2,1} \rangle &= -\frac{2c_3}{\Lambda'(\lambda)} \int \frac{h_{2,0}}{(\lambda + i\omega)(3\lambda + \lambda^* + 2i\omega)} d\omega \\ &+ \frac{2\pi K}{\Lambda'(\lambda)} \left(\int h_{1,0} d\omega \right) \int \frac{\psi}{(\lambda + i\omega)(3\lambda + \lambda^* + 2i\omega)} d\omega \\ &+ \frac{2\pi K}{\Lambda'(\lambda)} \int \frac{h_{1,0}}{(\lambda + i\omega)(3\lambda + \lambda^* + 2i\omega)} d\omega \\ &- \frac{2\pi K}{\Lambda'(\lambda)} \int \frac{h_{3,0}}{(\lambda + i\omega)(3\lambda + \lambda^* + 2i\omega)} d\omega. \end{aligned} \quad (\text{F.40})$$

Each integral of the right-hand-side is calculated by the partial fraction decomposition:

$$\begin{aligned} &\int \frac{h_{2,0}}{(\lambda + i\omega)(3\lambda + \lambda^* + 2i\omega)} d\omega \\ &= \frac{\pi K}{2} \left[\frac{1}{\lambda_R^3} \Lambda \left(\frac{3\lambda + \lambda^*}{2} \right) - \frac{1}{\lambda_R^2} \Lambda'(\lambda) - \frac{1}{2\lambda_R} \Lambda''(\lambda) \right], \end{aligned} \quad (\text{F.41})$$

$$\int \frac{\psi}{(\lambda + i\omega)(3\lambda + \lambda^* + 2i\omega)} d\omega = -\frac{1}{2\lambda_R^2} \Lambda \left(\frac{3\lambda + \lambda^*}{2} \right) + \frac{1}{2\lambda_R} \Lambda'(\lambda), \quad (\text{F.42})$$

$$\begin{aligned} &\int \frac{h_{1,0}}{(\lambda + i\omega)(3\lambda + \lambda^* + 2i\omega)} d\omega = \left(\int h_{1,0} d\omega \right) \left[\frac{1}{2\lambda_R^2} \Lambda \left(\frac{3\lambda + \lambda^*}{2} \right) - \frac{\Lambda(2\lambda + \lambda^*)}{4\lambda_R^2} \right] \\ &- \pi^2 K^2 \left[\frac{1}{2\lambda_R^4} \Lambda \left(\frac{3\lambda + \lambda^*}{2} \right) - \frac{1}{16\lambda_R^4} \Lambda(2\lambda + \lambda^*) - \frac{3}{8\lambda_R^3} \Lambda'(\lambda) - \frac{1}{8\lambda_R^2} \Lambda''(\lambda) \right] \\ &- c_3 \left[\frac{1}{8\lambda_R^3} \Lambda(2\lambda + \lambda^*) - \frac{1}{2\lambda_R^3} \Lambda \left(\frac{3\lambda + \lambda^*}{2} \right) + \frac{1}{4\lambda_R^2} \Lambda'(\lambda) \right], \end{aligned} \quad (\text{F.43})$$

$$\begin{aligned} &\int \frac{h_{3,0}}{(\lambda + i\omega)(3\lambda + \lambda^* + 2i\omega)} d\omega \\ &= \frac{\pi^2 K^2}{2} \left[-\frac{1}{\lambda_R^4} \Lambda \left(\frac{3\lambda + \lambda^*}{2} \right) + \frac{1}{\lambda_R^3} \Lambda'(\lambda) + \frac{1}{2\lambda_R^2} \Lambda''(\lambda) + \frac{1}{6\lambda_R} \Lambda'''(\lambda) \right]. \end{aligned} \quad (\text{F.44})$$

Appendix F.6. Calculation of c_7

For c_7 , we calculate $\int h_{1,1} d\omega$ and $\langle \tilde{\psi}, h_{2,2} \rangle$.

Appendix F.6.1. $\int h_{1,1} d\omega$ From Eq. Equation (F.19),

$$\begin{aligned} h_{1,1} &= \frac{K}{2} \frac{g(\omega)}{3\lambda + 2\lambda^* + i\omega} \int h_{1,1} d\omega - \pi K \left(\int h_{1,0} d\omega \right)^* \frac{h_{2,0}}{3\lambda + 2\lambda^* + i\omega} \\ &- \pi K \frac{h_{2,1}}{3\lambda + 2\lambda^* + i\omega} - (2c_3 + c_3^*) \frac{h_{1,0}}{3\lambda + 2\lambda^* + i\omega} - c_5 \frac{\psi}{3\lambda + 2\lambda^* + i\omega}. \end{aligned} \quad (\text{F.45})$$

Integrating over ω , we have

$$\begin{aligned} \Lambda(3\lambda + 2\lambda^*) \int h_{1,1} d\omega &= -\pi K \left(\int h_{1,0} d\omega \right)^* \int \frac{h_{2,0}}{3\lambda + 2\lambda^* + i\omega} d\omega \\ &- \pi K \int \frac{h_{2,1}}{3\lambda + 2\lambda^* + i\omega} d\omega - (2c_3 + c_3^*) \int \frac{h_{1,0}}{3\lambda + 2\lambda^* + i\omega} d\omega - c_5 \int \frac{\psi}{3\lambda + 2\lambda^* + i\omega} d\omega. \end{aligned} \quad (\text{F.46})$$

We calculate each of the integrals on the right hand side as follows:

$$\int \frac{h_{2,0}}{3\lambda + 2\lambda^* + i\omega} d\omega = \frac{\pi K}{2} \left(-\frac{1}{8\lambda_R^2} \Lambda(3\lambda + 2\lambda^*) + \frac{1}{2\lambda_R} \Lambda'(\lambda) \right), \quad (\text{F.47})$$

$$\begin{aligned} & \int \frac{h_{2,1}}{3\lambda + 2\lambda^* + i\omega} d\omega \\ &= -c_3 \pi K \left[\frac{1}{48\lambda_R^3} \Lambda(3\lambda + 2\lambda^*) - \frac{1}{3\lambda_R^3} \Lambda\left(\frac{3\lambda + \lambda^*}{2}\right) + \frac{1}{4\lambda_R^2} \Lambda'(\lambda) \right] \\ &+ 2\pi K \left(\int h_{1,0} d\omega \right) \left[-\frac{1}{24\lambda_R^2} \Lambda(3\lambda + 2\lambda^*) + \frac{1}{6\lambda_R^2} \Lambda\left(\frac{3\lambda + \lambda^*}{2}\right) \right] \\ &+ 2\pi K \left\{ \left(\int h_{1,0} d\omega \right) \left[-\frac{1}{12\lambda_R^2} \Lambda(3\lambda + 2\lambda^*) - \frac{1}{6\lambda_R^2} \Lambda\left(\frac{3\lambda + \lambda^*}{2}\right) \right] \right. \\ &\quad \left. + \frac{1}{4\lambda_R^2} \Lambda(2\lambda + \lambda^*) \right\} \end{aligned} \quad (\text{F.48})$$

$$\begin{aligned} & -\frac{\pi^2 K^2}{2} \left[-\frac{1}{96\lambda_R^4} \Lambda(3\lambda + 2\lambda^*) - \frac{1}{3\lambda_R^4} \Lambda\left(\frac{3\lambda + \lambda^*}{2}\right) + \frac{1}{8\lambda_R^4} \Lambda(2\lambda + \lambda^*) + \frac{1}{8\lambda_R^3} \Lambda'(\lambda) \right] \\ & -c_3 \left[\frac{1}{48\lambda_R^3} \Lambda(3\lambda + 2\lambda^*) + \frac{1}{6\lambda_R^3} \Lambda\left(\frac{3\lambda + \lambda^*}{2}\right) - \frac{1}{8\lambda_R^3} \Lambda(2\lambda + \lambda^*) \right] \Big\} \\ & -\pi^3 K^3 \left[-\frac{1}{192\lambda_R^4} \Lambda(3\lambda + 2\lambda^*) + \frac{1}{3\lambda_R^4} \Lambda\left(\frac{3\lambda + \lambda^*}{2}\right) - \frac{5}{16\lambda_R^3} \Lambda'(\lambda) - \frac{1}{8\lambda_R^2} \Lambda''(\lambda) \right], \\ & \int \frac{h_{1,0}}{3\lambda + 2\lambda^* + i\omega} d\omega = \left(\int h_{1,0} d\omega \right) \left[\frac{1}{2\lambda_R} \Lambda(3\lambda + 2\lambda^*) - \frac{1}{2\lambda_R} \Lambda(2\lambda + \lambda^*) \right] \\ & -\frac{\pi^2 K^2}{2} \left[\frac{1}{16\lambda_R^3} \Lambda(3\lambda + 2\lambda^*) - \frac{1}{4\lambda_R^3} \Lambda(2\lambda + \lambda^*) + \frac{1}{4\lambda_R^2} \Lambda'(\lambda) \right] \end{aligned} \quad (\text{F.49})$$

$$\begin{aligned} & -c_3 \left[-\frac{1}{8\lambda_R^2} \Lambda(3\lambda + 2\lambda^*) + \frac{1}{4\lambda_R^2} \Lambda(2\lambda + \lambda^*) \right], \\ & \int \frac{\psi}{3\lambda + 2\lambda^* + i\omega} d\omega = \frac{1}{4\lambda_R} \Lambda(3\lambda + 2\lambda^*). \end{aligned} \quad (\text{F.50})$$

Appendix F.6.2. $\langle \tilde{\psi}, h_{2,2} \rangle$ From Eq. Equation (F.23),

$$\begin{aligned} h_{2,2} &= -\frac{3c_3 + c_3^*}{2} \frac{h_{2,1}}{2\lambda + \lambda^* + i\omega} - c_5 \frac{h_{2,0}}{2\lambda + \lambda^* + i\omega} \\ &+ \pi K \left(\int h_{1,1} d\omega \right) \frac{\psi}{2\lambda + \lambda^* + i\omega} + \pi K \frac{h_{1,1}}{2\lambda + \lambda^* + i\omega} \\ &+ \pi K \left(\int h_{1,0} d\omega \right) \frac{h_{1,0}}{2\lambda + \lambda^* + i\omega} - \pi K \frac{h_{3,1}}{2\lambda + \lambda^* + i\omega} \\ &- \pi K \left(\int h_{1,0} d\omega \right)^* \frac{h_{3,0}}{2\lambda + \lambda^* + i\omega}. \end{aligned} \quad (\text{F.51})$$

Hence the inner product is

$$\begin{aligned}
\langle \tilde{\psi}, h_{2,2} \rangle &= -\frac{3c_3 + c_3^*}{2\Lambda'(\lambda)} \int \frac{h_{2,1}}{(2\lambda + \lambda^* + i\omega)(\lambda + i\omega)} d\omega \\
&\quad - \frac{c_5}{\Lambda'(\lambda)} \int \frac{h_{2,0}}{(2\lambda + \lambda^* + i\omega)(\lambda + i\omega)} d\omega \\
&\quad + \frac{\pi K \left(\int h_{1,1} d\omega \right)}{\Lambda'(\lambda)} \int \frac{\psi}{(2\lambda + \lambda^* + i\omega)(\lambda + i\omega)} d\omega \\
&\quad + \frac{\pi K}{\Lambda'(\lambda)} \int \frac{h_{1,1}}{(2\lambda + \lambda^* + i\omega)(\lambda + i\omega)} d\omega \\
&\quad + \frac{\pi K \left(\int h_{1,0} d\omega \right)}{\Lambda'(\lambda)} \int \frac{h_{1,0}}{(2\lambda + \lambda^* + i\omega)(\lambda + i\omega)} d\omega \\
&\quad - \frac{\pi K}{\Lambda'(\lambda)} \int \frac{h_{3,1}}{(2\lambda + \lambda^* + i\omega)(\lambda + i\omega)} d\omega \\
&\quad - \frac{\pi K \left(\int h_{1,0} d\omega \right)^*}{\Lambda'(\lambda)} \int \frac{h_{3,0}}{(2\lambda + \lambda^* + i\omega)(\lambda + i\omega)} d\omega.
\end{aligned} \tag{F.52}$$

We calculate the following seven integrals.

$$\begin{aligned}
&\int \frac{h_{2,1}}{(2\lambda + \lambda^* + i\omega)(\lambda + i\omega)} d\omega \\
&= -2c_3\pi K \left[\frac{1}{2\lambda_R^4} \Lambda \left(\frac{3\lambda + \lambda^*}{2} \right) - \frac{1}{16\lambda_R^4} \Lambda(2\lambda + \lambda^*) - \frac{3}{8\lambda_R^3} \Lambda'(\lambda) - \frac{1}{8\lambda_R^2} \Lambda''(\lambda) \right] \\
&\quad + 2\pi K \left(\int h_{1,0} d\omega \right) \left[-\frac{1}{2\lambda_R^3} \Lambda \left(\frac{3\lambda + \lambda^*}{2} \right) + \frac{1}{8\lambda_R^3} \Lambda(2\lambda + \lambda^*) + \frac{1}{4\lambda_R^2} \Lambda'(\lambda) \right] \\
&\quad + 2\pi K \left\{ \left(\int h_{1,0} d\omega \right) \left[\frac{1}{4\lambda_R^2} \Lambda'(2\lambda + \lambda^*) + \frac{1}{2\lambda_R^3} \Lambda \left(\frac{3\lambda + \lambda^*}{2} \right) - \frac{3}{8\lambda_R^3} \Lambda(2\lambda + \lambda^*) \right] \right. \\
&\quad \left. + \pi^2 K^2 \left[-\frac{1}{16\lambda_R^3} \Lambda''(\lambda) - \frac{1}{4\lambda_R^4} \Lambda'(\lambda) + \frac{1}{16\lambda_R^4} \Lambda'(2\lambda + \lambda^*) + \frac{1}{2\lambda_R^5} \Lambda \left(\frac{3\lambda + \lambda^*}{2} \right) \right. \right. \\
&\quad \quad \left. \left. - \frac{5}{32\lambda_R^5} \Lambda(2\lambda + \lambda^*) \right] \right. \\
&\quad \left. - c_3 \left[\frac{1}{8\lambda_R^3} \Lambda'(\lambda) - \frac{1}{8\lambda_R^3} \Lambda'(2\lambda + \lambda^*) + \frac{1}{4\lambda_R^4} \Lambda(2\lambda + \lambda^*) - \frac{1}{2\lambda_R^4} \Lambda \left(\frac{3\lambda + \lambda^*}{2} \right) \right] \right\} \\
&\quad - 2\pi^3 K^3 \left[-\frac{1}{2\lambda_R^5} \Lambda \left(\frac{3\lambda + \lambda^*}{2} \right) + \frac{1}{32\lambda_R^5} \Lambda(2\lambda + \lambda^*) + \frac{7}{16\lambda_R^4} \Lambda'(\lambda) + \frac{3}{16\lambda_R^3} \Lambda''(\lambda) \right. \\
&\quad \quad \left. + \frac{1}{24\lambda_R^2} \Lambda'''(\lambda) \right],
\end{aligned} \tag{F.53}$$

$$\begin{aligned}
&\int \frac{h_{2,0}}{(2\lambda + \lambda^* + i\omega)(\lambda + i\omega)} d\omega \\
&= \pi K \left(\frac{1}{8\lambda_R^3} \Lambda(2\lambda + \lambda^*) - \frac{1}{4\lambda_R^2} \Lambda'(\lambda) - \frac{1}{4\lambda_R} \Lambda''(\lambda) \right),
\end{aligned} \tag{F.54}$$

$$\int \frac{\psi}{(2\lambda + \lambda^* + i\omega)(\lambda + i\omega)} d\omega = -\frac{1}{4\lambda_R^2} \Lambda(2\lambda + \lambda^*) + \frac{1}{2\lambda_R} \Lambda'(\lambda), \tag{F.55}$$

$$\begin{aligned}
& \int \frac{h_{1,1}}{(2\lambda + \lambda^* + i\omega)(\lambda + i\omega)} d\omega = \\
& \left(\int h_{1,1} d\omega \right) \left[-\frac{1}{8\lambda_R^2} \Lambda(3\lambda + 2\lambda^*) + \frac{1}{4\lambda_R^2} \Lambda(2\lambda + \lambda^*) \right] \\
& -\pi^2 K^2 \left(\int h_{1,0} d\omega \right)^* \left[-\frac{1}{128\lambda_R^4} \Lambda(3\lambda + 2\lambda^*) + \frac{1}{16\lambda_R^4} \Lambda(2\lambda + \lambda^*) - \frac{3}{32\lambda_R^3} \Lambda'(\lambda) \right. \\
& \quad \left. - \frac{1}{16\lambda_R^2} \Lambda''(\lambda) \right] \\
& + 2\pi^2 K^2 c_3 \left[\frac{1}{768\lambda_R^5} \Lambda(3\lambda + 2\lambda^*) + \frac{1}{6\lambda_R^5} \Lambda\left(\frac{3\lambda + \lambda^*}{2}\right) - \frac{1}{32\lambda_R^5} \Lambda(2\lambda + \lambda^*) \right. \\
& \quad \left. - \frac{7}{64\lambda_R^4} \Lambda'(\lambda) - \frac{1}{32\lambda_R^3} \Lambda''(\lambda) \right] \\
& - 2\pi^2 K^2 \left(\int h_{1,0} d\omega \right) \left[-\frac{1}{192\lambda_R^4} \Lambda(3\lambda + 2\lambda^*) - \frac{1}{6\lambda_R^4} \Lambda\left(\frac{3\lambda + \lambda^*}{2}\right) \right. \\
& \quad \left. + \frac{1}{16\lambda_R^4} \Lambda(2\lambda + \lambda^*) + \frac{1}{16\lambda_R^3} \Lambda'(\lambda) \right] \\
& - 2\pi^2 K^2 \left\{ \left(\int h_{1,0} d\omega \right) \left[-\frac{1}{96\lambda_R^4} \Lambda(3\lambda + 2\lambda^*) + \frac{1}{6\lambda_R^4} \Lambda\left(\frac{3\lambda + \lambda^*}{2}\right) \right. \right. \\
& \quad \left. \left. - \frac{1}{8\lambda_R^4} \Lambda(2\lambda + \lambda^*) + \frac{1}{8\lambda_R^3} \Lambda'(2\lambda + \lambda^*) \right] \right. \\
& \quad \left. - \pi^2 K^2 \left[-\frac{1}{1536\lambda_R^6} \Lambda(3\lambda + 2\lambda^*) + \frac{1}{6\lambda_R^6} \Lambda\left(\frac{3\lambda + \lambda^*}{2}\right) - \frac{1}{16\lambda_R^6} \Lambda(2\lambda + \lambda^*) \right. \right. \\
& \quad \left. \left. + \frac{1}{32\lambda_R^5} \Lambda'(2\lambda + \lambda^*) - \frac{9}{128\lambda_R^5} \Lambda'(\lambda) - \frac{1}{64\lambda_R^4} \Lambda''(\lambda) \right] \right. \\
& \quad \left. - c_3 \left[\frac{1}{384\lambda_R^5} \Lambda(3\lambda + 2\lambda^*) - \frac{1}{6\lambda_R^5} \Lambda\left(\frac{3\lambda + \lambda^*}{2}\right) + \frac{3}{32\lambda_R^5} \Lambda(2\lambda + \lambda^*) \right. \right. \\
& \quad \left. \left. - \frac{1}{16\lambda_R^4} \Lambda'(2\lambda + \lambda^*) + \frac{1}{32\lambda_R^4} \Lambda'(\lambda) \right] \right\} \\
& + 2\pi^4 K^4 \left[-\frac{1}{3072\lambda_R^6} \Lambda(3\lambda + 2\lambda^*) - \frac{1}{6\lambda_R^6} \Lambda\left(\frac{3\lambda + \lambda^*}{2}\right) + \frac{1}{64\lambda_R^6} \Lambda(2\lambda + \lambda^*) \right. \\
& \quad \left. + \frac{35}{256\lambda_R^5} \Lambda'(\lambda) + \frac{7}{128\lambda_R^4} \Lambda''(\lambda) + \frac{1}{96\lambda_R^3} \Lambda'''(\lambda) \right] \\
& - (2c_3 + c_3^*) \left\{ \left(\int h_{1,0} d\omega \right) \left[\frac{1}{16\lambda_R^3} \Lambda(3\lambda + 2\lambda^*) - \frac{1}{4\lambda_R^2} \Lambda'(2\lambda + \lambda^*) \right] \right. \\
& \quad \left. - \pi^2 K^2 \left[\frac{1}{256\lambda_R^5} \Lambda(3\lambda + 2\lambda^*) + \frac{1}{16\lambda_R^5} \Lambda(2\lambda + \lambda^*) - \frac{1}{16\lambda_R^4} \Lambda'(2\lambda + \lambda^*) \right. \right. \\
& \quad \left. \left. - \frac{5}{64\lambda_R^4} \Lambda'(\lambda) - \frac{1}{32\lambda_R^3} \Lambda''(\lambda) \right] \right. \\
& \quad \left. - c_3 \left[-\frac{1}{64\lambda_R^4} \Lambda(3\lambda + 2\lambda^*) - \frac{1}{16\lambda_R^4} \Lambda(2\lambda + \lambda^*) + \frac{1}{8\lambda_R^3} \Lambda'(2\lambda + \lambda^*) + \frac{1}{16\lambda_R^3} \Lambda'(\lambda) \right] \right\} \\
& - c_5 \left[\frac{1}{32\lambda_R^3} \Lambda(3\lambda + 2\lambda^*) - \frac{1}{8\lambda_R^3} \Lambda(2\lambda + \lambda^*) + \frac{1}{8\lambda_R^2} \Lambda'(\lambda) \right], \tag{F.56}
\end{aligned}$$

$$\begin{aligned}
& \int \frac{h_{1,0}}{(2\lambda + \lambda^* + i\omega)(\lambda + i\omega)} d\omega = \left(\int h_{1,0} d\omega \right) \left[\frac{1}{4\lambda_R^2} \Lambda(2\lambda + \lambda^*) - \frac{1}{2\lambda_R} \Lambda'(2\lambda + \lambda) \right] \\
& - \pi^2 K^2 \left[\frac{3}{16\lambda_R^4} \Lambda(2\lambda + \lambda^*) - \frac{1}{8\lambda_R^3} \Lambda'(2\lambda + \lambda^*) - \frac{1}{4\lambda_R^3} \Lambda'(\lambda) - \frac{1}{8\lambda_R^2} \Lambda''(\lambda) \right] \quad (\text{F.57}) \\
& - c_3 \left[-\frac{1}{4\lambda_R^3} \Lambda(2\lambda + \lambda^*) + \frac{1}{4\lambda_R^2} \Lambda'(2\lambda + \lambda^*) + \frac{1}{4\lambda_R^2} \Lambda'(\lambda) \right],
\end{aligned}$$

$$\begin{aligned}
& \int \frac{h_{3,1}}{(2\lambda + \lambda^* + i\omega)(\lambda + i\omega)} d\omega \\
& = -3c_3 \pi^2 K^2 \left[-\frac{81}{64\lambda_R^5} \Lambda \left(\frac{4\lambda + \lambda^*}{3} \right) + \frac{1}{64\lambda_R^5} \Lambda(2\lambda + \lambda^*) + \frac{13}{16\lambda_R^4} \Lambda'(\lambda) \right. \\
& \quad \left. + \frac{1}{4\lambda_R^3} \Lambda''(\lambda) + \frac{1}{24\lambda_R^2} \Lambda'''(\lambda) \right] \\
& + 3\pi^2 K^2 \left(\int h_{1,0} d\omega \right) \left[\frac{27}{32\lambda_R^4} \Lambda \left(\frac{4\lambda + \lambda^*}{3} \right) - \frac{1}{32\lambda_R^4} \Lambda(2\lambda + \lambda^*) - \frac{1}{2\lambda_R^3} \Lambda'(\lambda) \right. \\
& \quad \left. - \frac{1}{8\lambda_R^2} \Lambda''(\lambda) \right] \\
& - 6c_3 \pi^2 K^2 \left[\frac{81}{64\lambda_R^5} \Lambda \left(\frac{4\lambda + \lambda^*}{3} \right) - \frac{1}{2\lambda_R^5} \Lambda \left(\frac{3\lambda + \lambda^*}{2} \right) + \frac{1}{64\lambda_R^5} \Lambda(2\lambda + \lambda^*) \right. \\
& \quad \left. - \frac{3}{8\lambda_R^4} \Lambda'(\lambda) - \frac{1}{16\lambda_R^3} \Lambda''(\lambda) \right] \\
& + 6\pi^2 K^2 \left(\int h_{1,0} d\omega \right) \left[-\frac{27}{32\lambda_R^4} \Lambda \left(\frac{4\lambda + \lambda^*}{3} \right) + \frac{1}{2\lambda_R^4} \Lambda \left(\frac{3\lambda + \lambda^*}{2} \right) \right. \\
& \quad \left. - \frac{1}{32\lambda_R^4} \Lambda(2\lambda + \lambda^*) + \frac{1}{8\lambda_R^3} \Lambda'(\lambda) \right] \\
& + 6\pi^2 K^2 \left(\int h_{1,0} d\omega \right) \left[\frac{27}{64\lambda_R^4} \Lambda \left(\frac{4\lambda + \lambda^*}{3} \right) - \frac{1}{2\lambda_R^4} \Lambda \left(\frac{3\lambda + \lambda^*}{2} \right) \right. \\
& \quad \left. + \frac{13}{256\lambda_R^4} \Lambda(2\lambda + \lambda^*) - \frac{1}{16} \Lambda'(2\lambda + \lambda^*) \right] \quad (\text{F.58}) \\
& - 6\pi^4 K^4 \left[\frac{243}{256\lambda_R^6} \Lambda \left(\frac{4\lambda + \lambda^*}{3} \right) - \frac{1}{2\lambda_R^6} \Lambda \left(\frac{3\lambda + \lambda^*}{2} \right) + \frac{9}{64\lambda_R^6} \Lambda(2\lambda + \lambda^*) \right. \\
& \quad \left. - \frac{1}{64\lambda_R^5} \Lambda'(2\lambda + \lambda^*) - \frac{7}{32\lambda_R^5} \Lambda'(\lambda) - \frac{1}{32\lambda_R^4} \Lambda''(\lambda) \right] \\
& - 6c_3 \pi^2 K^2 \left[-\frac{81}{128\lambda_R^5} \Lambda \left(\frac{4\lambda + \lambda^*}{3} \right) + \frac{1}{2\lambda_R^5} \Lambda \left(\frac{3\lambda + \lambda^*}{2} \right) - \frac{11}{128\lambda_R^5} \Lambda(2\lambda + \lambda^*) \right. \\
& \quad \left. + \frac{1}{32\lambda_R^4} \Lambda'(2\lambda + \lambda^*) + \frac{1}{16\lambda_R^4} \Lambda'(\lambda) \right] \\
& - 6\pi^4 K^4 \left[-\frac{243}{128\lambda_R^6} \Lambda \left(\frac{4\lambda + \lambda^*}{3} \right) + \frac{1}{2\lambda_R^6} \Lambda \left(\frac{3\lambda + \lambda^*}{2} \right) - \frac{1}{128\lambda_R^6} \Lambda(2\lambda + \lambda^*) \right. \\
& \quad \left. + \frac{25}{32\lambda_R^5} \Lambda'(\lambda) + \frac{3}{16\lambda_R^4} \Lambda''(\lambda) + \frac{1}{48\lambda_R^3} \Lambda'''(\lambda) \right] \\
& - 3\pi^4 K^4 \left[\frac{243}{128\lambda_R^6} \Lambda \left(\frac{4\lambda + \lambda^*}{3} \right) - \frac{1}{128\lambda_R^6} \Lambda(2\lambda + \lambda^*) - \frac{5}{4\lambda_R^5} \Lambda'(\lambda) \right. \\
& \quad \left. - \frac{13}{32\lambda_R^4} \Lambda''(\lambda) - \frac{1}{12\lambda_R^3} \Lambda'''(\lambda) - \frac{1}{96\lambda_R^2} \Lambda''''(\lambda) \right],
\end{aligned}$$

$$\int \frac{h_{3,0}}{(2\lambda + \lambda^* + i\omega)(\lambda + i\omega)} d\omega = \pi^2 K^2 \left[-\frac{1}{16\lambda_R^4} \Lambda(2\lambda + \lambda^*) + \frac{1}{8\lambda_R^3} \Lambda'(\lambda) + \frac{1}{8\lambda_R^2} \Lambda''(\lambda) + \frac{1}{12\lambda_R} \Lambda'''(\lambda) \right]. \quad (\text{F.59})$$

Appendix G. Discussion on the line III using c_7

The amplitude equation is obtained perturbatively, and therefore, we have to be careful if the perturbation is valid or not. Looking back the equation for the amplitude $\sigma = |A|^2$, Equation (35), we require the inequalities

$$|\text{Re}(c_3(K))\sigma_*| \gg |\text{Re}(c_5(K))\sigma_*^2| \gg |\text{Re}(c_7(K))\sigma_*^3|. \quad (\text{G.1})$$

These inequalities must be satisfied at $K = K_Q$ in Fig. 9 to capture the three roots of $G_3(\sigma)$. Thus we set σ_* as the smallest root of $G_3(\sigma)$ at $K = K_Q$. The value of σ_* can be approximated by

$$\sigma'_* = -\frac{\text{Re}(c_3(K_{Q'}))}{2\text{Re}(c_5(K_{Q'}))}, \quad (\text{G.2})$$

where $K_{Q'}$ is the vanishing point of the discriminant of $G_2(\sigma)$. To check one of the inequalities, the ratio

$$R_{7/3} = \frac{|\text{Re}(c_7(K_{Q'}))(\sigma'_*)^3|}{|\text{Re}(c_3(K_{Q'}))\sigma'_*|} \quad (\text{G.3})$$

is reported in Fig. G1. The ratio $R_{7/3}$ is larger than 1 in almost the whole plane of (γ_1, Ω) , and therefore, the perturbation up to the third order, $G_3(\sigma)$, is not valid except for a certain limited region.

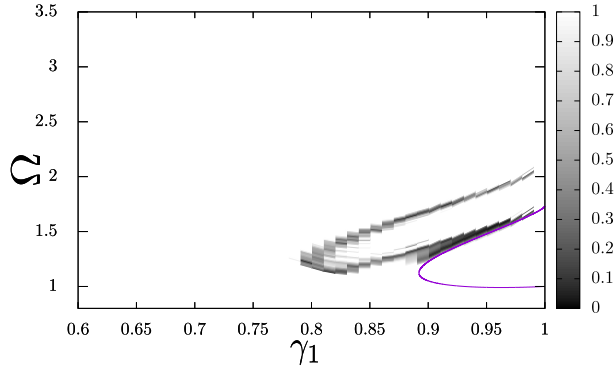


Figure G1. Heat map of $R_{7/3}$, Equation (G.3), on the parameter space (γ_1, Ω) . The perturbation condition is satisfied only around the line II (magenta solid line).

Let us also check if the criterion with using $G_2(\sigma)$ is valid or not. Algebraic computations give

$$\frac{|\text{Re}(c_5(K_{Q'}))(\sigma'_*)^2|}{|\text{Re}(c_3(K_{Q'}))\sigma'_*|} = \frac{1}{2} < 1. \quad (\text{G.4})$$

Therefore, the perturbation is not bad at the point $K_{Q'}$ at which we give the criterion for the domain E.

References

- [1] J. Pantaleone, Synchronization of metronomes, *Am. J. Phys.* **70**, 992 (2002).
- [2] H. M. Smith, Synchronous flashing of fireflies, *Science* **82**, 151 (1935).
- [3] J. Buck and E. Buck, Mechanism of rhythmic synchronous flashing of fireflies, *Science* **159**, 1319 (1968).
- [4] I. Aihara, T. Mizumoto, T. Otsuka, H. Awano, K. Nagira, H. G. Okuno and K. Aihara, Spatio-Temporal Dynamics in Collective Frog Choruses Examined by Mathematical Modeling and Field Observations, *Sci. Rep.* **4**, 3891 (2014).
- [5] K. Wiesenfeld, P. Colet and S. H. Strogatz, Synchronization Transitions in a Disordered Josephson Series Array, *Phys. Rev. Lett.* **76**, 404 (1996).
- [6] K. Wiesenfeld, P. Colet and S. H. Strogatz, Frequency locking in Josephson arrays: Connection with the Kuramoto model, *Phys. Rev. E* **57**, 1563 (1998).
- [7] A. T. Winfree, Biological Rhythms and the Behavior of Populations of Coupled Oscillators, *J. Theoret. Biol.* **16**, 15 (1967).
- [8] Y. Kuramoto, Self-entertainment of a population of coupled non-linear oscillators, *International Symposium on Mathematical Problems in Theoretical Physics, Lecture Notes in Physics* **39**, 420 (1975).
- [9] S. H. Strogatz, From Kuramoto to Crawford: exploring the onset of synchronization in populations of coupled oscillators, *Physica* **143D**, 1 (2000).
- [10] H. Chiba, A proof of the Kuramoto conjecture for a bifurcation structure of the infinite-dimensional Kuramoto model, *Ergod. Theory Dyn. Syst.* **35**, 762 (2015).
- [11] E. A. Martens, E. Barreto, S. H. Strogatz, E. Ott, P. So, and T. M. Antonsen, Exact results for the Kuramoto model with a bimodal frequency distribution, *Phys. Rev. E* **79**, 026204 (2009).
- [12] Y. Terada, K. Ito, T. Aoyagi, and Y. Y. Yamaguchi, Nonstandard transition in the Kuramoto model: a role of asymmetry in natural frequency distributions, *J. Stat. Mech.* (2017) 0134403.
- [13] D. Hansel, G. Mato and C. Meunier, Phase Dynamics for Weakly Coupled Hodgkin-Huxley Neurons, *Europhys. Lett.* **23**, 367 (1993).
- [14] I. Z. Kiss, Y. Zhai and J. L. Hudson, Predicting Mutual Entrainment of Oscillators with Experiment-Based Phase Models, *Phys. Rev. Lett.* **94**, 248301 (2005).
- [15] I. Z. Kiss, Y. Zhai and J. L. Hudson, Characteristics of Cluster Formation in a Population of Globally Coupled Electrochemical Oscillators: An Experiment-Based Phase Model Approach, *Prog. Theor. Phys. Suppl.* **161**, 99 (2006).
- [16] M. Komarov and A. Pikovsky, Multiplicity of Singular Synchronous States in the Kuramoto Model of Coupled Oscillators, *Phys. Rev. Lett.* **111**, 204101 (2013).
- [17] M. Komarov and A. Pikovsky, The Kuramoto model of coupled oscillators with a bi-harmonic coupling function, *Physica D* **289**, 18 (2014).
- [18] E. Ott and T. M. Antonsen, Low dimensional behavior of large systems of globally coupled oscillators, *Chaos* **18**, 037113 (2008).
- [19] E. Ott and T. M. Antonsen, Long time evolution of phase oscillator systems, *Chaos* **19**, 023117 (2009).
- [20] J. D. Crawford, Amplitude Expansions for Instabilities in Populations of Globally-Coupled Oscillators, *J. Statist. Phys.* **74**, 1047 (1994).
- [21] J. D. Crawford, Scaling and Singularities in the Entrainment of Globally Coupled Oscillators, *Phys. Rev. Lett.* **74**, 4341 (1995).
- [22] J. Barré and D. Métivier, Bifurcations and Singularities for Coupled Oscillators with Inertia and Frustration, *Phys. Rev. Lett.* **117**, 214102 (2016).
- [23] J. D. Crawford, Universal Trapping Scaling on the Unstable Manifold for a Collisionless Electrostatic Mode, *Phys. Rev. Lett.* **73**, 656 (1994).
- [24] J. D. Crawford, Amplitude equations for electrostatic waves: Universal singular behavior in the limit of weak instability, *Phys. Plasmas* **2**, 97 (1995).
- [25] Y. Terada, K. Ito, R. Yoneda, T. Aoyagi and Y. Y. Yamaguchi, A role of asymmetry in linear response of globally coupled oscillator systems, arXiv:1802.08383.
- [26] C. Lancellotti, On the Vlasov Limit for Systems of Nonlinearly Coupled Oscillators without Noise, *Transp. Theory Stat.* **34**, 523 (2004).
- [27] S. H. Strogatz, R. E. Mirollo and P. C. Matthews, Coupled Nonlinear Oscillators below the Synchronization Threshold: Relaxation by Generalized Landau Damping, *Phys. Rev. Lett.* **68**, 2730 (1992).
- [28] J. Barré and Y. Y. Yamaguchi, Small traveling clusters in attractive and repulsive Hamiltonian mean-field models, *Phys. Rev. E* **79**, 036208 (2009).
- [29] H. Sakaguchi and Y. Kuramoto, A Soluble Active Rotator Model Showing Phase Transitions via

- Mutual Entrainment, *Prog. Theor. Phys.* **76**, 576 (1986).
- [30] O. E. Omel'chenko and M. Wulfrum, Nonuniversal Transitions to Synchrony in the Sakaguchi-Kuramoto Model, *Phys. Rev. Lett.* **109**, 164101 (2012).
 - [31] M. K. S. Yeung and S. H. Strogatz, Time Delay in the Kuramoto Model of Coupled Oscillators, *Phys. Rev. Lett.* **82**, 648 (1999).
 - [32] E. Montbrió, D. Pazó and J. Schmidt, Time delay in the Kuramoto model with bimodal frequency distribution, *Phys. Rev. E* **74**, 056201 (2006).
 - [33] S. Ogawa, Spectral and formal stability criteria of spatially inhomogeneous stationary solutions to the Vlasov equation for the Hamiltonian mean-field model, *Phys. Rev. E* **87**, 062107 (2013).